

Global and non-global parameters of horizontal branch morphology of globular clusters ¹

A. P. Milone^{2,3,4}, A. F. Marino², A. Dotter², J. E. Norris², H. Jerjen², G. Piotto^{5,7}, S. Cassisi⁶, L. R. Bedin⁷, A. Recio Blanco⁸, A. Sarajedini⁹, M. Asplund², M. Monelli^{3,4}, A. Aparicio^{3,4}

ABSTRACT

The horizontal branch (HB) morphology of globular clusters (GCs) is mainly determined by metallicity. However, the fact that GCs with almost the same metallicity exhibit different HB morphologies demonstrates that at least one more parameter is needed to explain the HB morphology. It has been suggested that one of these should be a *global* parameter that varies from GC to GC, and the other a *non-global* parameter that varies within the GC.

In this study we provide empirical evidence corroborating this idea. We used the photometric catalogs obtained with the Advanced Camera for Surveys (ACS) of the *Hubble Space Telescope (HST)* and analyse the CMDs of 74 GCs. The HB morphology of our sample of GCs has been investigated on the basis of the two new parameters $L1$ and $L2$ that measure the distance between the RGB and the coolest part of the HB, and the color extension of the HB, respectively.

²Research School of Astronomy and Astrophysics, The Australian National University, Cotter Road, Weston, ACT, 2611, Australia; milone@mso.anu.edu.au, amarino@mso.anu.edu.au, jen@mso.anu.edu.au, jerjen@mso.anu.edu.au, martin@mso.anu.edu.au

³Instituto de Astrofísica de Canarias, E-38200 La Laguna, Tenerife, Canary Islands, Spain; monelli@iac.es, aparicio@iac.es

⁴Department of Astrophysics, University of La Laguna, E-38200 La Laguna, Tenerife, Canary Islands, Spain

⁵Dipartimento di Fisica e Astronomia, ‘Galileo Galilei’ Università di Padova, Vicolo dell’Osservatorio 3, Padova I-35122, Italy; giampaolo.piotto@unipd.it

⁶INAF-Osservatorio Astronomico di Collurania, via Mentore Maggini, I-64100 Teramo, Italy; cassisi@oa-teramo.inaf.it

⁷INAF-Osservatorio Astronomico di Padova, Vicolo dell’Osservatorio 5, I-35122 Padua, Italy; luigi.bedin@oapd.inaf.it

⁸Observatoire de la Côte d’Azur, UMR Cassiopee, B. P. 4229, 06304 Nice Cedex 04, France; alejandra.recio-blanco@oca.eu

⁹Department of Astronomy, University of Florida, 211 Bryant Space Science Center, Gainesville, FL 32611, USA; ata@astro.ufl.edu

We find that $L1$ correlates with both metallicity and age, whereas $L2$ most strongly correlates with the mass of the hosting GC. The range of helium abundance among the stars in a GC, characterised by ΔY and associated with the presence of multiple stellar populations, has been estimated in a few GCs to date. In these GCs we find a close relationship among ΔY , GC mass, and $L2$. We conclude that age and metallicity are the main *global* parameters while the range of helium abundance within a GC is the main *non-global* parameter defining the HB morphology of Galactic GCs.

Subject headings: stars: abundances — stars: Population II — globular clusters — general

1. Introduction

Since the early 1950s, metallicity has been considered the main parameter that determines the horizontal-branch (HB) morphology in globular clusters (GCs; e.g., Arp 1952). Within a few years, evidence that some GCs with similar metallicity exhibit different HB morphologies suggested that at least a second parameter (2ndP) is required to properly characterise the HB morphology of GCs (e.g. Sandage & Wallerstein 1960; van den Bergh 1965). Since then, the so called 2ndP problem has been widely investigated by many authors.

Several candidates have been suggested as possible 2ndPs, including mass loss (e.g. Peterson 1982; Catelan 2000), stellar rotation (e.g. Mengel & Gross 1976; Fusi-Pecci & Renzini 1978), planetary systems (e.g. Soker 1998; Siess & Livio 1999), magnetic fields (e.g. Rood & Seitzer 1981), and GC ellipticity (Norris 1983) but a comprehensive picture is still lacking. Age (e.g. Searle & Zinn 1978; Catelan & de Fretais Pacheco 1993; Lee et al. 1994), GC central density (e.g. Fusi-Pecci et al. 1993), GC mass (e.g. Recio-Blanco et al. 2006), and helium abundance (e.g. Sandage & Wildey 1967; van den Bergh 1967) are among the best candidates. We refer the reader to the papers by Freeman & Norris (1981), Catelan et al. (2009), Dotter et al. (2010), Gratton et al. (2010), and references therein for reviews on HB stars and the 2ndP phenomenon in GCs.

The study of GCs has changed dramatically in recent years due to the overwhelming evidence for the existence of multiple stellar populations in GCs. In this way of thinking a GC is made up of a first generation of stars, formed from the GC’s primordial gas cloud, and at least one later generation, formed from a dilution of the primordial gas and the chemical yields of the high- and intermediate-mass stars of the first generation.

¹Based on observations with the NASA/ESA *Hubble Space Telescope*, obtained at the Space Telescope Science Institute, which is operated by AURA, Inc., under NASA contract NAS 5-26555.

The possibility of GC self-enrichment, especially as it relates to enhanced helium, as cause for the variation of the HB morphology has been investigated by several authors, as multiple stellar populations with different helium abundance can indeed explain features such as tails and multimodalities in the HBs of GCs (e.g. Ferraro et al. 1998; D’Antona et al. 2002, 2005; Piotto et al. 2007; Caloi & D’Antona 2008; Gratton et al. 2010). The idea of a connection between multiple stellar populations and HB morphology arose in the early 1980s, when pioneering papers showed that the cyanogen distribution is closely connected to the shape of the HB (e.g. Norris 1981; Norris et al. 1981; Smith & Norris 1993) this result has been confirmed by recent studies of HB stars.

In this context the GC M4 is exemplary. High-resolution spectroscopy of red-giant branch (RGB) stars reveals that this GC hosts two stellar populations with different Na and O abundances while photometry reveals two RGBs in the U versus $U - B$ color-magnitude diagram (CMD). The HB of M4 is bimodal and well-populated on both sides of the RR Lyrae gap (Marino et al. 2008). The bimodality in Na and O is also present among the HB stars. Blue-HB stars belong to the second population and are O-poor and Na-rich, while red HB stars are first population (Marino et al. 2008, 2011a). Similar analysis of Na and O in HB stars in other GCs show that first generation HB stars preferentially populate the reddest HB segment while second generation HB stars tend towards bluer colors (Villanova et al. 2009, Gratton et al. 2011, 2012, 2013), Lovisi et al. 2012, Marino et al. 2013a). More recently, Marino et al. (2013b) inferred from direct spectroscopic measurements that Na-rich HB stars of NGC 2808 are also strongly helium enhanced.

Several factors influence HB morphology and it is difficult to disentangle the different effects. An important point in the study of the 2ndP is that the metric used to characterise HB morphology is not objective: the chosen way of representing the HB stars in a GC as a number has a non-trivial influence on the results of the investigation. Most studies to date adopt a single HB morphology metric. Different studies, using different metrics, can easily reach conflicting conclusions about the identity of the 2ndP.

Consider the following two examples. Recio-Blanco et al. (2006) defined their HB morphology metric as the maximum effective temperature along the HB and found that more massive GCs tend to have hotter HBs. Dotter et al. (2010) measured the median color difference between the HB and the RGB at the level of the HB ($\Delta(V - I)$) from *Hubble Space Telescope* (HST) Advanced Camera for Surveys (ACS) photometry of sixty GCs, and demonstrated that, after the metallicity dependence is accurately removed, $\Delta(V - I)$ correlates most strongly with GC age.

Dotter et al. (2010, see their Figure 2) compared $\Delta(V - I)$ with the widely-used HB Type index²

²Defined as $(B - R)/(B + V + R)$, where B, R, and V are the numbers of blue HB, red HB, and variables stars. It measures the relative contributions of stars bluer or redder than the RR Lyrae instability strip, and is variously known by the definition, HB Type, or HB Ratio (HBR).

and the maximum effective temperature along the HB as defined by Recio-Blanco et al. (2006). The comparison shows that $\Delta(V - I)$ and HB Type are closely correlated but that $\Delta(V - I)$ and Recio-Blanco et al.’s maximum HB temperature are not: they have very different sensitivities. It is not surprising that a metric sensitive to the extremes of the distribution correlates with a different (second) parameter than a metric sensitive to the center of the distribution. The problem is that 2ndP studies typically select only one HB morphology metric and the conclusions are influenced by that choice.

We suggest that a more effective way to proceed is to consider more than one HB morphology metric simultaneously. For maximum effect, these metrics should share a simple, common definition but not be closely correlated with each other. The motivation for this approach is not only based on the practicalities outlined above. Freeman & Norris (1981) argued that two parameters, one global and one local, may be needed to fully describe the observed variations in HB morphology. The local parameter is one that varies within a single GC; the global parameter is one that varies among the GC population.

The aim of this paper is an empirical investigation of the parameters governing the HB morphology of GCs, in the context of the classical 2ndP phenomenon. To do this we use the homogeneous high-accuracy photometry from GO 10775, the Advanced Camera for Surveys (ACS) Survey of Galactic GCs (P.I. A. Sarajedini, Sarajedini et al. 2007), and from GO 11586 (P.I. A. Dotter, Dotter et al. 2011) and additional photometry from *HST* to re-investigate the HB morphology in GCs in light of the new findings on multiple stellar populations in GCs and of the global versus non-global parameter idea by Freeman & Norris (1981). The paper is organised as follows. Sect. 2 describes the observational data. Sect. 3 introduces the quantities adopted to describe the HB morphology and defines the new HB morphology parameters $L1$ and $L2$. Sect. 4 assembles a variety of GC parameters from the literature. Sect. 5 compares these parameters with $L1$ and $L2$. Sect. 6 discusses our findings in the context of similar studies in the literature. Finally, we summarise our findings in Sect. 7.

2. The data sample

We used the photometric catalogs obtained from GO 10775 and GO 11586 that include homogeneous photometric and astrometric measurements for 65 and 6 GCs, respectively. For each of them, the dataset consists of one short and four or five long exposures in the F606W and F814W bandpasses. We excluded from GO 10775 three GCs: Pal 1 and E 3 for the lack of identifiable HB stars, and Pal 2 for the extreme differential reddening. The details concerning the data, the data reduction, and the calibration are given in Anderson et al. (2008) and Dotter et al. (2011).

In their study of the HB in GCs, Dotter et al. (2010) emphasised the importance of properly accounting for the outer Halo, where the 2ndP is more evident. To increase the number of outer-Halo GCs, we have extended the GO 10775 and GO 11586 to six more GCs: AM-1, Eridanus, NGC 2419, Pal 3, Pal 4, Pal 14. For both Pal 4 and Pal 14 we used 2×60s F606W and 2×80s F814W ACS/WFC images from GO 10622 (PI. Dolphin), while for NGC 2419 we used the F606W and F814W magnitudes published by di Criscienzo et al. (2011). These data have been reduced as already described in Anderson et al. (2008), Dotter et al. (2011), and di Criscienzo et al. (2011). For Pal 3 and Eridanus we used ground-based V , I photometry from

Stetson et al. (1999), and for AM-1 Wide Field Planetary Camera 2 (WFPC2) photometry from Dotter et al. (2008) in F555W and F814W. Photometry for these three GCs has been transformed into F606W and F814W ACS/WFC bands by using the relationships given in Sirianni et al. (2005).

Photometry has been corrected for spatial photometric zero-point variation both due to differential reddening and small inaccuracies in the PSF model (Anderson et al. 2008). For most GCs we used the corrected magnitudes and colors published by Milone et al. (2012b, 59 GCs), Piotto et al. (2012, NGC 6752), di Criscienzo et al. (2011, NGC 2419), and Bellini et al. (2010, ω Centauri). For the remaining GCs we corrected the photometry following the procedure described in Milone et al. (2012b).

3. Two new parameters to describe the HB morphology: $L1$ and $L2$

To investigate the HB morphology, we defined two quantities: $L1$, the color difference between the RGB and the coolest border the HB, and $L2$, the color extension of the HB³.

The procedure to determine $L1$ and $L2$ is illustrated in Fig. 1 for the case of NGC 5904 (M 5). We selected by eye a sample of HB stars that we plotted as blue circles in the lower panel, and a sample of RGB stars that we represented with red points. The RGB sample includes all the RGB stars with luminosity differing by less than ± 0.1 F606W mag from the mean level of the HB ($F606W_{\text{HB}}$), where the $F606W_{\text{HB}}$ values are taken from Dotter et al. (2010, Table 1). The histograms of the normalised $m_{\text{F606W}} - m_{\text{F814W}}$ color distribution for the HB and RGB sample are

³We emphasise that we have not introduced $L1$ and $L2$ because we believe that they are more (or less) efficient than any other diagnostic previously used in the study of the HB morphology. Nevertheless, results of the empirical analysis presented in this paper will show that $L1$ and $L2$ are useful tools to shed light on the 2ndP phenomenon. Any search for the best diagnostic of the HB morphology is obviously outside the scope of our paper and is possibly naive: one would need to understand a-priori which parameters determine HB morphology, and then compare the sensitivity of $L1$, $L2$, and the other diagnostics of the HB morphology used in literature with these parameters.

shown in the upper panel and colored blue and red, respectively. We have defined two points on the HB, P_A and P_B , whose colors correspond to the fourth and the ninety-sixth percentile of the color distribution of HB stars. The color of the third point P_C is assumed as the median color of RGB stars. $L1$ is defined as the color difference between P_C and P_B , and $L2$ as the color difference between P_B and P_A . Uncertainties on P_A , P_B , P_C , $L1$ and $L2$ are estimated for each GC by bootstrapping with replacements performed 1,000 times on both the RGB and the HB. The error bars indicate one standard deviation (68.27th percentile) of the bootstrapped measurements. The colors of P_A , P_B , P_C , the values of $L1$ and $L2$, and the corresponding errors, are listed in Tab. 1.

RR Lyrae have been observed at random phases and some of them could lie outside the instability strip. Similarly to what has been done in previous papers on the second parameter (e.g. Gratton et al. 2010, Dotter et al. 2010) we included in our analysis only those RR Lyrae that are close to the instability strip. In the appendix we investigate the impact of excluding RR Lyrae that might be out of the instability strip in the determination of $L1$ and $L2$ and conclude that this does not affect the conclusions of our paper.

4. GC parameters

In the next section we shall compare the $L1$ and $L2$ HB morphology indicators with the physical and morphological GC parameters described here. Metallicity ($[Fe/H]$), absolute visual magnitude (M_V), central velocity dispersion (σ_V), ellipticity (ϵ), central concentration (c), core relaxation timescale (τ_c), half-mass relaxation timescale (τ_{hm}), logarithm of central stellar density (ρ_0), central surface brightness (μ_V), and Galactocentric distance (R_{GC}) are extracted from the 2010 edition of the Harris (1996) catalog. The specific frequency of RR Lyrae variables ($S_{RR\ Lyrae}$) is taken from the 2003 edition of the Harris (1996) catalog. The fraction of binary stars have been measured by Milone et al. (2012b,c) in the core of the GC (f_{bin}^C), in the region between the core and the half-mass radius (f_{bin}^{C-HM}), and outside the half-mass radius (f_{bin}^{oHM}). We also use age and helium measurements, and some indicators of light-element variations, as discussed in detail in Sect. 4.1 and Sect. 4.2, respectively.

4.1. Age

We adopt GC age measurements from De Angeli et al. (2005), Marín-Franch et al. (2009), VandenBerg et al. (2013), and Leaman et al. (2013), and Dotter et al. (2010, 2011). De Angeli et al. (2005) determined ages for 55 GCs by measuring the difference between the HB and the turnoff in two internally photometrically homogeneous *HST* and ground-based databases (Piotto

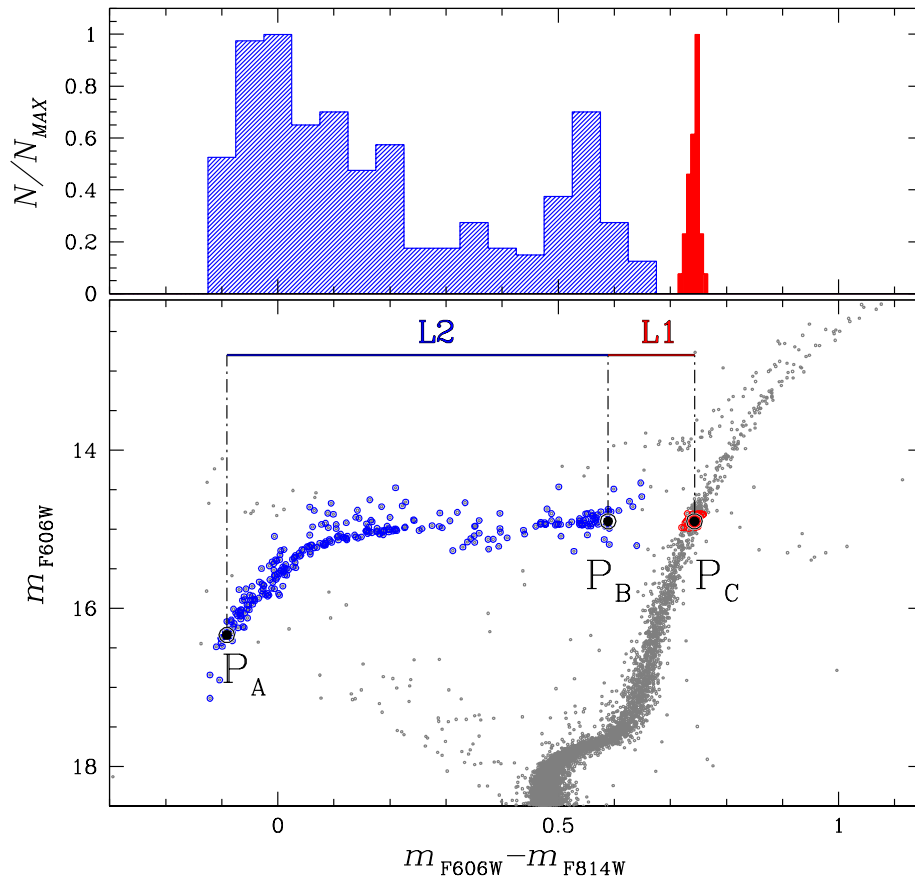


Fig. 1.— *Upper panel*: Normalised histogram color distribution of stars in the HB (blue histogram) and RGB sample (red histogram) for NGC 5904. The RGB sample includes all the RGB stars with luminosity differing by less than ± 0.1 F606W mag from the mean level of the HB. The two samples of HB and RGB stars are colored blue and red, respectively in the lower-panel CMD, where we also show the points P_A , P_B , P_C and the $L1$ and $L2$ segments (see text for details).

et al. 2002; Rosemberg et al. 1999). Among the GCs studied by De Angeli et al. (2005), 41 are in common with the ACS data.

Marín-Franch et al. (2009) used the same GO 10775 photometric database analysed in the present paper to estimate relative ages for 64 GCs that are included in our dataset with internal uncertainties of 2%-7%. Ages are derived by comparing the observed relative position of the GC main sequence turnoff (MSTO) with an isochrones-based grid of MSTOs.

More recently, Vandenberg et al. (2013) and Leaman et al. (2013) compared Victoria-Regina isochrones with photometry from Sarajedini et al. (2007) and Anderson et al. (2008) to derive ages

for 61 GCs that are also included in our paper. To do this, they adopted an improved version of the classical ‘vertical method’, which is based on the luminosity difference between the MSTO and the zero-age HB.

Age estimates by Dotter et al. (2010, 2011) are determined by using isochrone fitting to the CMDs for 59 of the GCs studied in this paper; note that these authors omitted 6 GCs present in the ACS Survey of Galactic GCs due to the presence of multiple stellar populations with either large helium variation or double subgiant branch (SGB). For the remainder of the ACS Survey GCs (NGC 1851, NGC 2808, NGC 6388, NGC 6441, NGC 6656, and NGC 6715) we calculated ages following the same recipes from Dotter and collaborators. We obtained: 11.00 ± 0.50 Gyr (NGC 1851), 11.50 ± 0.75 Gyr (NGC 2808), 11.75 ± 0.75 Gyr (NGC 6388), 12.00 ± 1.00 Gyr (NGC 6441), 13.50 ± 1.00 Gyr (NGC 6656), and 13.25 ± 0.75 Gyr (NGC 6715).

NGC 1851, NGC 6388, NGC 6656, and NGC 6715 each exhibit a double SGB (Milone et al. 2008; Marino et al. 2009; Piotto et al. 2012) that is consistent with two groups of stars that have either an age difference of 1-2 Gyrs or almost the same age and different C+N+O abundance (Cassisi et al. 2008; Ventura et al. 2009). High-resolution spectroscopy of SGB and RGB stars in NGC 6656 showed that the faint SGB of this GC is indeed made of C+N+O enhanced stars (Marino et al. 2011a; Alves-Brito et al. 2012) and that, by accounting for the chemical content of the two stellar groups, isochrone fitting of the double SGB indicates that their ages do not differ by more than ~ 300 Myr (Marino et al. 2012). Large star-to-star C+N+O variations, with faint SGB-stars being also enhanced in C+N+O, have been also observed in NGC 1851 (Yong et al. 2009 and in preparation) even if this result is not confirmed by Villanova et al. (2010). For GCs with a double SGB we assume the age obtained from fitting the bright SGB. To distinguish between GCs with single or bimodal SGBs, the statistical analysis of the relation between HB-morphology and age presented in Sect. 5 will be presented with and without these double-SGB GCs.

When investigating the effect of age on HB morphology a challenge comes from the fact that the population of Milky Way GCs mainly consists of old objects. Young clusters are hence important in the present investigation as any effect of age on the HB morphology would be better identified when comparing clusters with large age differences. In order to better sample the Galactic GC population at all Galactocentric distances, Dotter et al. (2010, 2011) expanded the sample studied by Marín-Franch et al. (2009) to include several more-distant GCs: AM-1 and Pal 14 (Dotter et al. 2008); Pal 3, Pal 4, and Eridanus (Stetson et al. 1999), and IC 4499, Pal 5, Pyxis, and Ruprecht 106 (Dotter et al. 2011). It come out that several of them are also young clusters.

Ages from Dotter and collaborators are available for 73 GCs, but only 61, 41, and 61 of them are included in the age compilations published by Marín-Franch et al. (2009), De Angeli et al. (2005), and by VandenBerg et al. (2013) and Leaman et al. (2013), respectively. Since the sample by Dotter and collaborators is the most complete and is based on the best dataset available, we

began by using their ages to investigate possible relations with $L1$ and $L2$. Although the other age compilations include a smaller GC sample, they can be used to demonstrate that our conclusions do not rely on a particular set of ages.

Another challenge comes from age errors that can be as large as 1.25 Gyr for the Dotter et al. (2010, 2011) sample. To minimize the impact of error measurements, our conclusions are based on the average properties of groups of GCs that will be defined in Sect. 5.1.

4.2. Light-element and helium variations

Our analysis makes use of several indicators of the intracluster light-element variations as well as of measurements of the helium differences among the multiple stellar populations in GCs. Some of these parameters have been defined several decades ago and widely discussed in the context of the 2ndP phenomenon while others have been introduced more recently.

Norris (1987) defined the ratio (R_{CN}) between CN-strong and CN-weak stars and provided R_{CN} measurements for a sample of 12 GCs, which was increased to 16 by Smith & Mateo (1990). The interquartile range of the [O/Na] ratio, $\text{IQR}[\text{O/Na}]$, can be considered as another indicator of the internal light-element variation to quantify the extension of the sodium-oxygen anticorrelation (Carretta et al. 2006). This parameter is available for 24 GCs: for 14 GCs, namely NGC 104, NGC 1904, NGC 2808, NGC 3201, NGC 4590, NGC 5904, NGC 6171, NGC 6218, NGC 6254, NGC 6388, NGC 6441, NGC 6809, NGC 6838, and NGC 7078, we used the $\text{IQR}[\text{O/Na}]$ values listed by Carretta et al. (2010a). For the other 10 GCs, we have calculated $\text{IQR}[\text{O/Na}]$ by using oxygen and sodium abundances available in the literature. We obtained $\text{IQR}[\text{O/Na}]=0.61$ and 0.67 for NGC 288 and NGC 362, respectively (Shetrone & Keane 2000); $\text{IQR}[\text{O/Na}]=0.68$ for NGC 1851 (Villanova et al. 2010); $\text{IQR}[\text{O/Na}]=0.54$ and 1.04 for NGC 5272 and NGC 6205, respectively (Snedden et al. 2004); $\text{IQR}[\text{O/Na}]=0.28$ for NGC 6397 (Lind et al. 2011); $\text{IQR}[\text{O/Na}]=1.16$ for NGC 6715 (Carretta et al. 2010a); $\text{IQR}[\text{O/Na}]=0.91$ for NGC 6752 (Yong et al. 2008); $\text{IQR}[\text{O/Na}]=0.49$, 0.67 , and 1.07 for NGC 6121, NGC 6656, and NGC 5139, respectively (Marino et al. 2008, 2011b,a).

In their survey of multiple stellar populations in GCs, Monelli et al. (2013) defined the photometric index $c_{\text{UBI}}=(U - B)-(B - I)$ and found that all the GCs they analysed show a multimodal or spread RGB in the V versus c_{UBI} diagram, with the c_{UBI} value of each star being related to its light element abundances. The c_{UBI} index width of the RGB (W_{RGB}) is listed by Monelli et al. (2013) for 22 GCs.

Some stars in GCs have light-element abundance similar to halo-field stars of the same metallicity (e.g. Kraft 1994). It is widely accepted that these stars constitute the first stellar population and can be distinguished from the other GC stars either on the basis of their abundance

of C, N, Na, O or their position in the CMD. For 47 Tuc, NGC 6397, NGC 6752, NGC 288 we adopted the fraction of first-population stars with respect to the total population (f_{POPI}) determined from photometric studies (Milone et al. 2012c,d, 2013; Piotto et al. 2013). For NGC 2808, and NGC 6121 we used the fractions derived by Marino et al. (2008) and Marino et al. (2013b), and for NGC 3201, NGC 4590, NGC 5272, NGC 5904, NGC 6171, NGC 6205, NGC 6218, NGC 6254, NGC 6388, NGC 6496, NGC 6838, NGC 7078, and NGC 7079 we used the value given by Carretta et al. (2010b).

While the quantities R_{CN} , $\text{IQR}[\text{O/Na}]$, and W_{RGB} are mainly related to the internal variations of light-elements, recent analysis based on multi-wavelength photometry made it possible to estimate the helium difference between stellar populations in a single GC. These studies have revealed that the CMD of a GC is typically composed of intertwined sequences, the separate identities of which can be followed continuously from the MS up to the RGB. These sequences are associated with stellar populations with different light-element and helium abundances (e.g. Milone et al. 2012d,a). The comparison of the observed multi-color difference between the different MSs and RGBs with colors obtained from appropriate theoretical stellar atmospheres provides an estimate of the maximum helium difference (ΔY) between the stellar populations that is not based on HB stars. Although this technique has been applied to only a few GCs to date, we shall use the available ΔY measurements, summarised in Tab. 2, to investigate possible relations with HB morphology in the next section.

While ΔY indicates the maximum internal variation in helium, the R-parameter (R) defined by Iben (1968) as the number ratio of HB to RGB stars brighter than the HB level is sensitive to the initial helium content of GCs. At a given metallicity, a higher initial He-content implies a brighter HB and, in turn, a lower number of RGB stars. In this paper we used the values of R determined by Salaris et al. (2004). Gratton et al. (2010) introduced a similar parameter $R' = N_{\text{HB}}/N'_{\text{RGB}}$, where N_{HB} is the number of HB stars, N'_{RGB} the number of RGB stars brighter than $V(\text{HB})+1$, and $V(\text{HB})$ is the V magnitude of the HB taken from the Harris (1996) catalog. Gratton and collaborators used the R-parameter method Iben (1968) to derive He abundance for GCs ($Y(R')$). As suggested by the referee, we extend our analysis to the $Y(R')$ values provided by Gratton et al. (2010).

5. Relationship between HB-morphology and globular cluster parameters.

In this Section we investigate the correlations among $L1$, $L2$, and several physical and morphological parameters of their host GCs. Specifically, relations with metallicity, absolute magnitude, and age are discussed in Sect. 5.1, 5.2, and 5.3 respectively. Section 5.4 investigates the correlations with the internal variations of the light elements and helium, while relations between $L1$ and $L2$ and the other parameters introduced in Sect. 4 are analysed in Sect. 5.5.

When we compare two variables, as we do in the next section for $L1$, $L2$, and $[\text{Fe}/\text{H}]$, we use the Spearman’s rank correlation coefficient r , to estimate the statistical dependence between the two. Uncertainties in r are estimated by means of bootstrapping statistics. We generated 1,000 resamples of the observed dataset, of equal size, and for each resample (i), (which is generated by random sampling with replacement from the original dataset) we estimated r_i . We considered the dispersion of the r_i measurements (σ_r) as indicative of robustness of r and provide the number of included GCs (N).

5.1. Metallicity

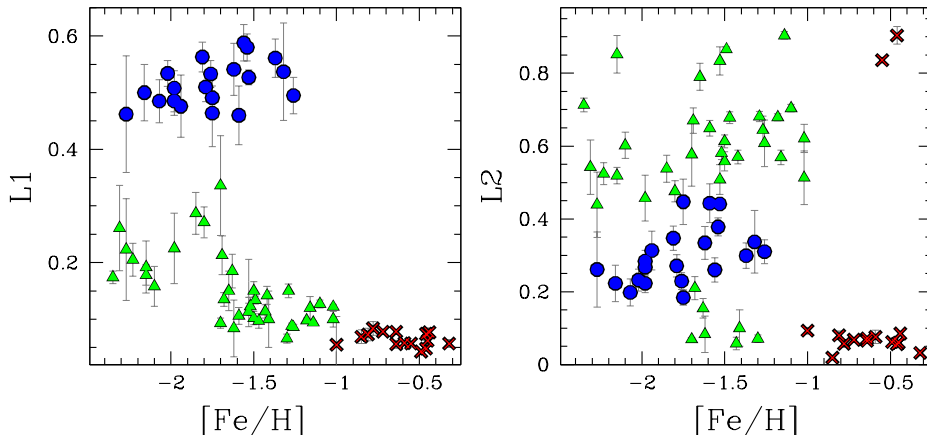


Fig. 2.— *Left panel:* $L1$ versus GC metallicity for the 72 GCs studied in this work. The G1, G2, and G3 GCs are colored red, green, and blue, respectively. *Right panel:* $L2$ against metallicity.

The left panel of Fig. 2 shows $L1$ against the GC metallicity. An inspection of this plot reveals that all the metal-rich GCs have small $L1$ values and, hence, red-HBs. At lower metallicities, there are GCs with almost the same iron abundance and yet different $L1$ values⁴. This reflects the basic 2ndP phenomenon. Indeed, if all of the GCs followed the same relation in the $L1$ versus $[\text{Fe}/\text{H}]$ plane, we would assume that metallicity alone is sufficient to determine $L1$. The fact that we observe clusters with the same $[\text{Fe}/\text{H}]$ but different $L1$ values, indicates that, apart from metallicity, at least one more parameter is at work.

⁴The fact that $L1$ possesses a dependence on metallicity is expected from theory. Similarly, it is well known from theory that several other parameters may determine HB morphology and hence can affect the values of $L1$ and $L2$. This paper is an attempt to investigate those parameters that are actually at work by following a fully-empirical approach.

Our finding that the analysed GCs populate distinct regions in the $L1$ versus $[\text{Fe}/\text{H}]$ plane, and that the 2ndP phenomenon is absent among the majority of metal-rich GCs motivated us to define three groups of GCs as follows:

1. The first group, G1, includes all the metal-rich GCs ($[\text{Fe}/\text{H}] \geq -1.0$);
2. the second, G2, is made of GCs with $[\text{Fe}/\text{H}] < -1.0$ and $L1 \leq 0.4$; and
3. the remaining GCs with $L1 > 0.4$ belong to G3.

Since the 2ndP phenomenon is absent among the majority of G1 GCs, we will also consider a group that includes all the GCs in G2 and G3, hereafter G2+G3. The statistical analysis presented in the following will be provided for all the GCs together, as well as for the different groups separately.

There is a significant anticorrelation between $L1$ and $[\text{Fe}/\text{H}]$ among G2 GCs, with a Spearman’s rank correlation coefficient $r_{G2} = -0.70$ ($\sigma_{r,G2} = 0.08$, $N_{G2} = 38$) that drops to -0.88 if we consider G1 and G2 GCs together, an even stronger correlation. The Spearman’s correlation coefficients and the corresponding σ_r values are listed in Tab. 3 for the groups of GCs defined above. There is no correlation between $L2$ and $[\text{Fe}/\text{H}]$, either for G1 or G3 GCs.

Apart from NGC 6388 and NGC 6441, all G1 GCs host a purely red HB and have $L2$ values smaller than the majority of the other GCs. In G2 and G3 GCs metallicity is not responsible for the extension of the HB ($L2$) as shown in the right panel of Fig. 2.

5.2. Absolute Magnitude

The left panel of Fig. 3 shows that there is no significant correlation between $L1$ and the GC absolute luminosity for any of the groups of GCs defined above. In contrast, both G2 and G3 GCs exhibit significant anti-correlations between $L2$ and the absolute GC magnitude, which relates to the GC mass assuming all GCs have roughly the same mass-to-light ratio. This is shown in the right panel of Fig. 3, where we plot $L2$ as a function of M_V . The Spearman’s rank correlation coefficient is $r_{G2} = -0.89$ ($\sigma_{r,G2} = 0.05$, $N = 38$), and $r_{G3} = -0.71$ ($\sigma_{r,G3} = 0.13$, $N_{G3} = 21$) for the G2 and G3 samples, respectively, $r_{G2+G3} = -0.80$ ($\sigma_{r,G2+G3} = 0.06$, $N_{G2+G3} = 59$) for G2+G3 GCs.

5.3. Age

Histograms of the age distributions for G1, G2, and G3 GCs are shown in the upper panels of Fig. 4 for the age measurements from Dotter et al. (2010, 2011, left panel) and Marín-Franch

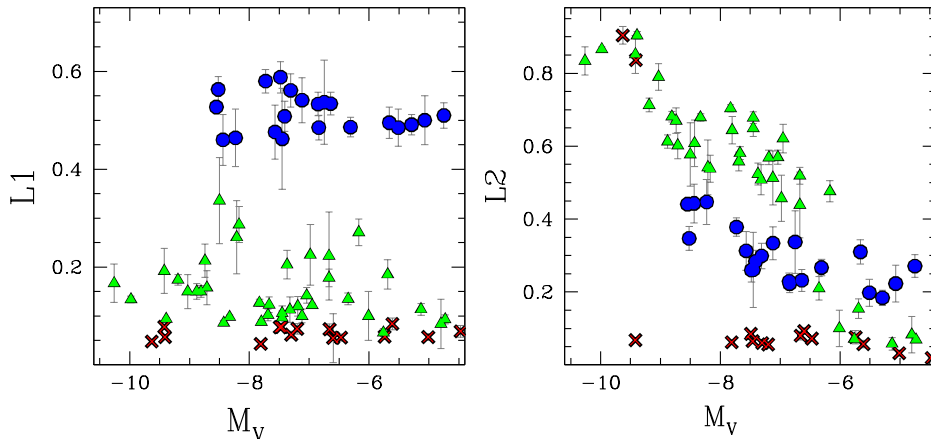


Fig. 3.— $L1$ (left panel) and $L2$ (right panel) as a function of GC absolute magnitude.

et al. (2009, right panel), and in Fig. 5 for the age measurements of De Angeli et al. (2005, left panel) and VandenBerg et al. (2013) and Leaman et al. (2013, right panel). On average, G3 GCs are systematically older than G2 GCs, and this result is independent of the adopted age scale. Specifically, independently from the four adopted age scales, on average, G2 GCs are younger than G3 ones by ~ 1 Gyr with G3 GCs clustered around the value of ~ 13 Gyrs, and G2 GCs spanning a wider age interval. The mean ages of G2 and G3 GCs are listed in Tab. 4.

$L1$ is plotted as a function of GC age in the middle panels of Figs. 4 and 5. There is a positive correlation between age and $L1$ for G2 GCs, with older G2 GCs having, on average, greater $L1$ values. The Spearman coefficient is high $r_{G2} \geq 0.70$, except when we adopt ages from Marín-Franch et al. (2009) indicating that in the latter case the significance level is low⁵.

As a further check we have divided GCs into three sub-groups with almost the same metallicity. We have defined a metal poor ($[\text{Fe}/\text{H}] < -1.7$), a metal intermediate ($-1.7 < [\text{Fe}/\text{H}] < -1.4$), and a metal rich ($[\text{Fe}/\text{H}] > -1.4$) group, and investigate age- $L1$ relation for GCs in each of them. Results are listed in Tab. 4. In all the cases, G3 GCs are systematically older even if, especially for metal-poor GCs, the statistical significance of the measured age difference is marginal, but we are limited by small number statistics. The fact that G3 GCs are systematically older than G2 GCs and the presence of significant correlation between age and $L1$ for G2 GCs indicate that GC age is partly responsible for the color distance between the RGB and the reddest part of the HB, being

⁵As pointed out by the referee, there are three G3 GCs which, according to Marín-Franch et al. (2009) are younger than ~ 12.25 Gyrs. Their ages are in agreement with the average age of G3 GCs only to within 1.5 - 2.5σ . We are not able to say if this difference is due to measurement errors or is intrinsic.

metallicity the other parameter for L1 extension⁶.

There is no significant correlation between $L2$ and age as shown in the lower panels of Fig. 4 and 5. GCs with a double or multimodal SGB, namely NGC 1851, NGC 6388, NGC 6656, and NGC 6715 have been excluded from the statistical analysis above. As discussed in Sect. 4.1, the large fraction of faint-SGB stars observed in these GCs can affect the age measurements. For completeness we provide in Tab. 3 the values of the Spearman’s rank correlation coefficients to estimate the statistical significance of $L1$, $L2$ and age correlations, together with results for the whole sample of GCs. The main results of this section remain unchanged when the GCs above are included in the analysis.

5.4. Helium and light elements

As mentioned in Sect. 1, the recent findings that in some GCs groups of stars with different light element abundances populate different HB segments strongly suggest that certain aspects of HB morphology may be strictly connected with multiple populations. To further investigate this scenario, in Figs. 6, 7, and 8 we show the relations between $L1$ and $L2$ and those quantities indicating intracluster chemical variations, which we introduced in Sect. 4.2. As shown in Figs. 6, 7, there is no significant correlation between $L1$ and W_{RGB} , $\text{IQR}([\text{O}/\text{Na}])$, or R_{CN} , f_{POPI} , nor between $L2$ and W_{RGB} , and f_{POPI} . No significant correlations are observed between $L1$, $L2$ and R or $Y(R')$. A mild correlation between $L2$ and $Y(R')$ can not be ruled out for G2 GCs ($r_{\text{G2}}=0.44$, $\sigma_{r,\text{G2}}=0.21$).

Figure 7 also shows that on average GCs with extended HBs have more extended Na-O anticorrelations, as demonstrated by the significant correlation between $L2$ and $\text{IQR}([\text{O}/\text{Na}])$ obtained for GCs in both G2 and G3. This result confirms the findings by Carretta et al. (2007) and Gratton et al. (2010). Among G2 GCs, those with large CN-strong and CN-weak populations ($R_{\text{CN}} > 2$) have, on average a more extended HB. The small number of G2 and G3 GCs where R_{CN} measurements are available prevents us from making any strong conclusion on the significance of the correlation with $L1$ and $L2$.

Theoretical models predict that star-to-star light-element variations observed in GC stars are associated with helium differences that lead to HB stars with different masses because of the well-known inverse relationship between helium abundance and stellar mass for fixed metallicity and

⁶ Gratton et al. (2010) also derived ages for a subsample of the clusters studied in the present paper. To determine these ages, they used stellar masses derived from isochrones that include ages from Marín-Franch et al. (2009) and De Angeli et al. (2005) already analysed in this paper. In addition, the way these ages are derived is closely related to the HB morphology. For these reasons we prefer to avoid to use them in the context of this paper. Nevertheless, we verified that our conclusions remain unchanged when ages from Gratton et al. (2010) are used.

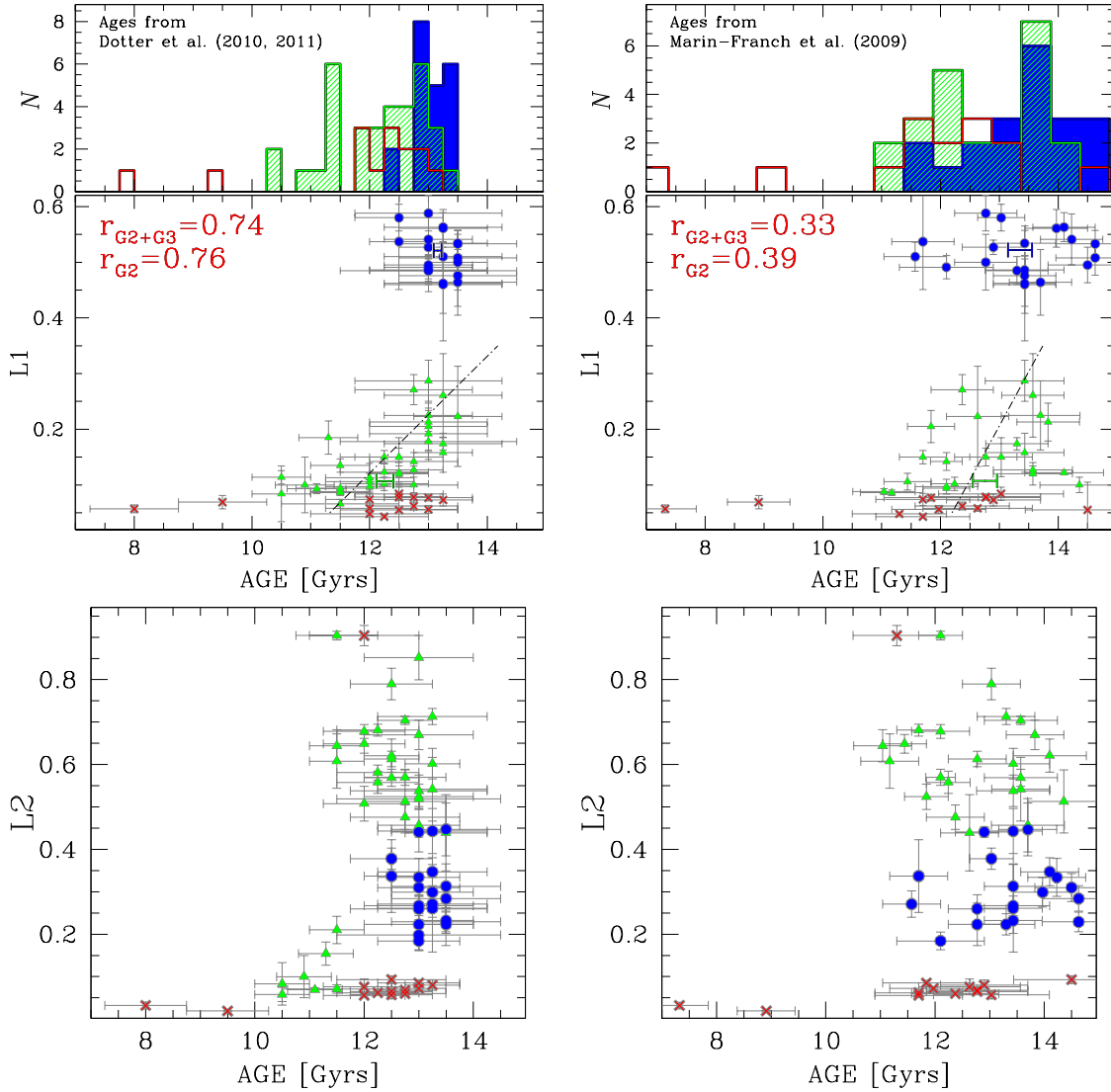


Fig. 4.— $L2$ (lower panels) and $L1$ (middle panels) against age. The histograms of age distribution for the G1 (red), G2 (green), and G3 (blue) GCs are plotted in the upper panel. In the left and right panels we used age measurements from Dotter et al. (2010, 2011) and Marín-Franch et al. (2009), respectively. Black dashed-dotted lines in the middle panel are the best-fitting straight lines for the G2 sample. The Spearman's coefficients r_{G2} and r_{G2+G3} are also indicated.

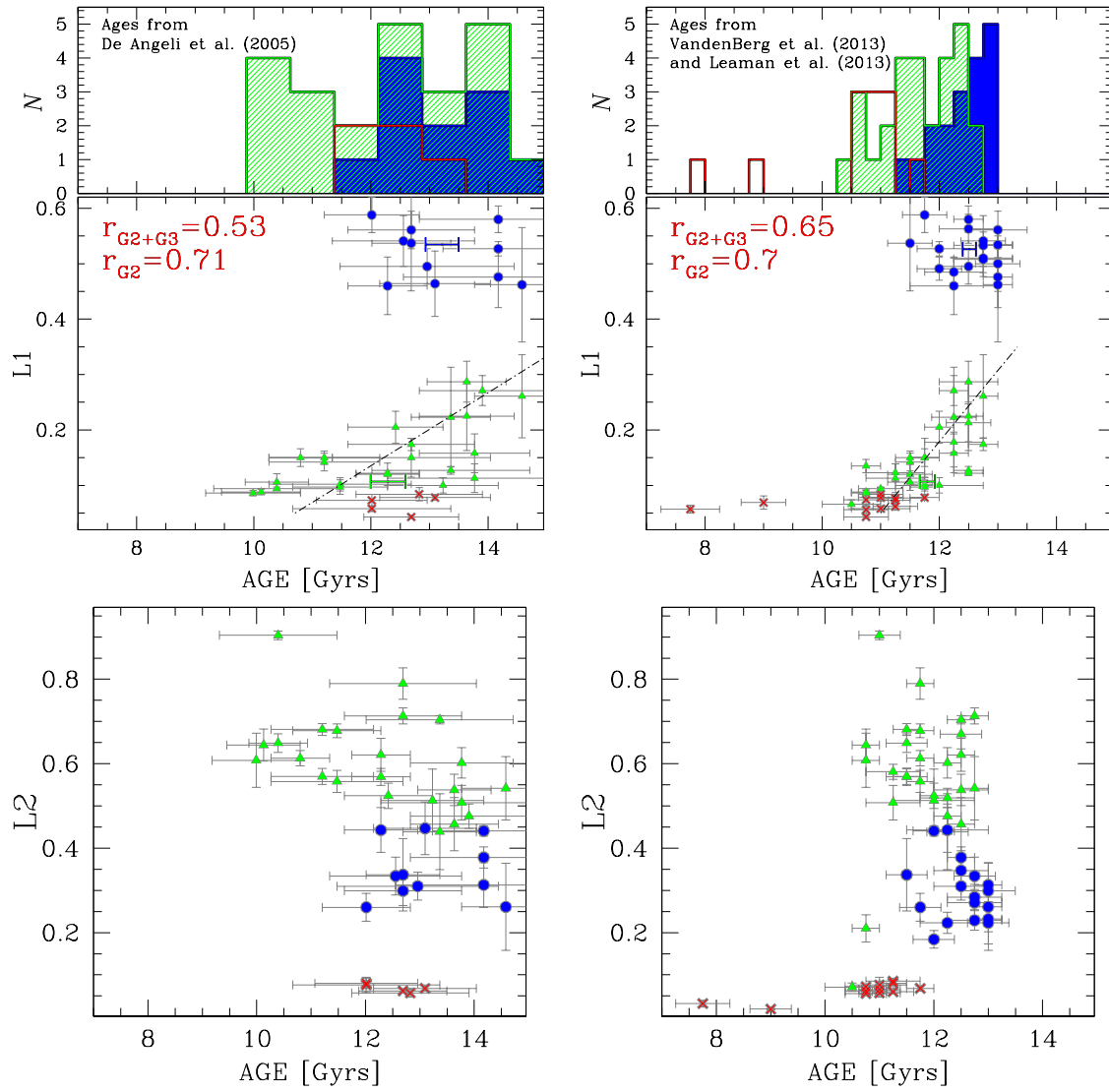


Fig. 5.— As in Fig. 4, but for age measurements from De Angeli et al. (2005, left panels) and for ages derived by Vandenberg et al. (2013) and Leaman et al. (2013, right panels).

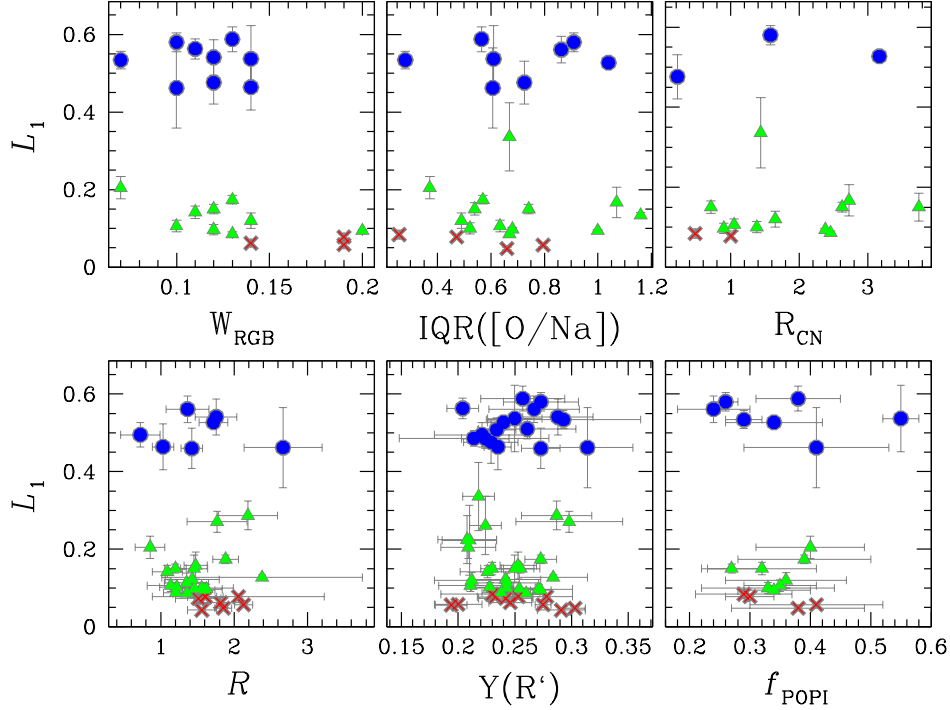


Fig. 6.— *Upper panels:* L_1 as a function of the width of the RGB in the c_{UBI} index (left), the interquartile range of [O/Na] ratio (middle), and the ratio between CN-strong and CN-weak stars (right). *Lower panels:* L_1 as a function of the R-parameter, that is the number ratio of HB to RGB stars brighter than the HB level (left), the helium abundance inferred by Gratton et al. (2010) from the Iben (1968) method based on the R-parameter (middle), and the fraction of first-population stars (right).

age (e.g. Ventura & D’Antona 2005 and references therein).⁷ The relation between L_1 , L_2 and the maximum internal helium difference measured from MS studies is plotted in Fig. 8. The tight correlation between L_2 ($r_{\text{G2+G3}}=0.89$, $\sigma_{r,\text{G2+G3}}=0.17$, $N_{\text{G2+G3}}=7$) and the small corresponding value of σ_r for G2+G3 clusters confirms theoretical indications that helium-enhanced stellar population are responsible of the HB extension.

⁷The helium content of a star affects its location along the HB as follows. When compared with helium-normal stars ($Y \sim 0.25$) of the same age and metallicity, He-enhanced stars have shorter main sequence lifetimes, and hence smaller masses at the main sequence turn-off for a fixed age. Assuming the He-normal and He-enhanced stars lose a similar amount of mass on the RGB, the He-enriched stars will have a smaller H-rich envelope on the HB and, thus, populate a hotter, bluer portion of the HB than the He-normal stars (e.g. Cassisi et al. 2012).

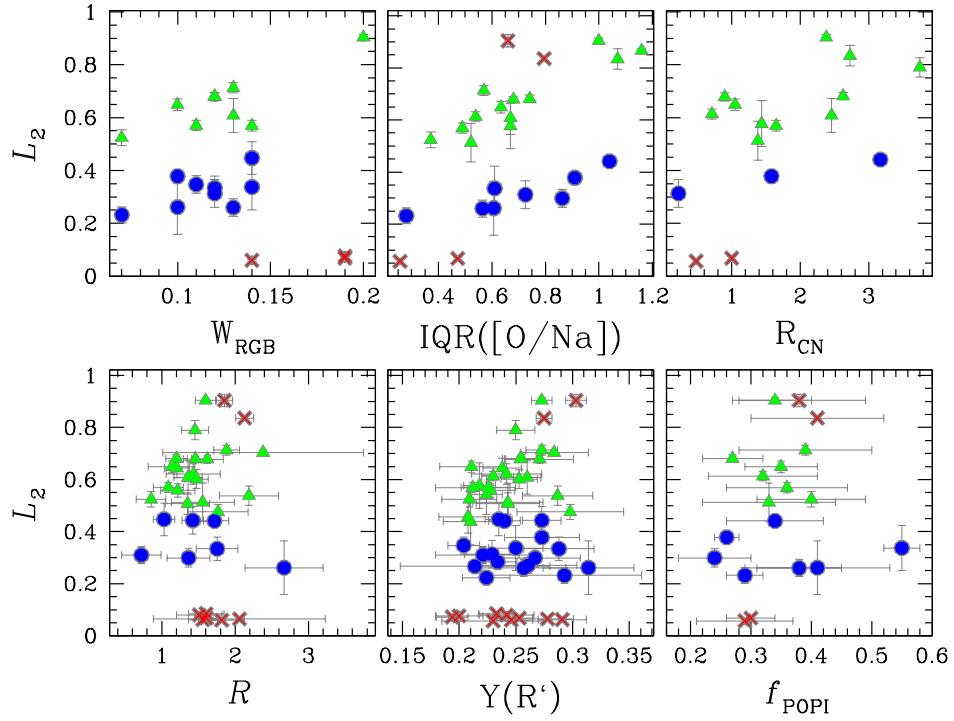


Fig. 7.— As in Fig. 6, but for L_2 .

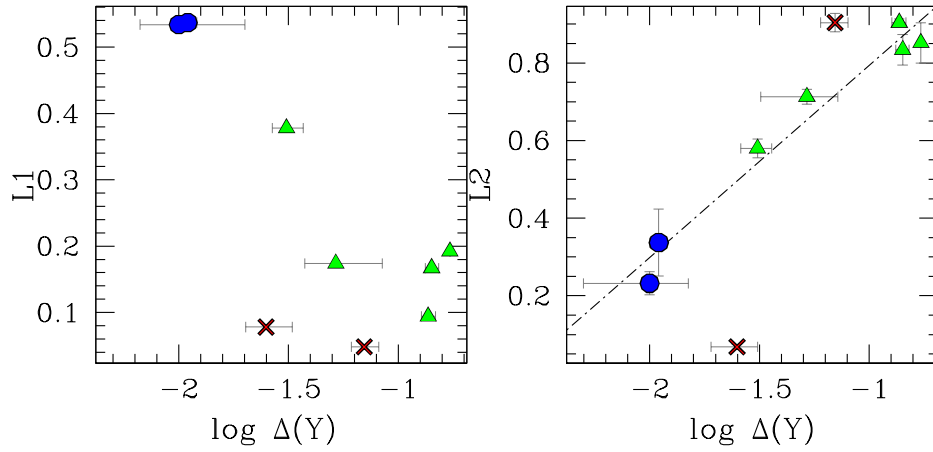


Fig. 8.— L_1 (left panel) and L_2 (right panel) as a function of the logarithm of the maximum helium difference among stellar populations in GCs. The black line is the best-fitting straight line for G2+G3 GCs.

5.5. Relationships with other parameters of the host globular clusters

Figure 9 shows other monovariate relations involving $L1$. There is no significant correlation between $L1$ and central velocity dispersion, King (1962) model central concentration, central brightness, central density, core and half mass relaxation time, GC ellipticity, Galactocentric distance, and binary fraction. This is confirmed by the values of the Spearman’s correlation coefficient listed in Tab. 3.

In Fig. 10 we see that $L2$ correlates with ρ and σ_v for G2 and G3 GCs, and anticorrelates with μ_v and $f_{\text{bin}}^{\text{C,C-HM,oHM}}$ for each group of GCs, even if the anticorrelation is less or not significant for the G2+G3 sample. These results are not unexpected as these quantities also correlate with GC mass (Djorgovski & Maylan 1994).

6. Comparison with the literature

According to Gratton et al. (2010), in the ADS data base there are more than two hundreds papers dedicated to the 2ndP phenomenon. Hence, any comparison here with the wide literature on the HB 2ndP can only be very far from complete. In this section we discuss some of the more relevant results. We refer the reader to review papers (e.g. Freeman & Norris 1981; Catelan 2009) and references therein for a complete view on this topic.

As already mentioned in Sect. 1, works on HB morphology in GCs make use of different HB metrics. In Fig. 11 and 12, we compare $L1$ and $L2$ with other quantities used to parametrize HB morphology. The parameter to describe HB morphology that is mostly used in literature is the HB Type index or HBR (see Sect. 1). Figures 11 and 12 compare $L1$ and $L2$ with HBR. There is a linear correlation between $L1$ and HBR for G2 GCs, and then HBR saturates for G1 and for G3 GCs. $L2$ does not correlate with HBR.

The wide literature on the 2ndP includes several works, similar to the present investigation, that are based on a fully-observational approach, together with others that also use a series of theoretical assumptions. A recent example of the latter is the paper by Gratton et al. (2010), in which the authors used *HST*/WFPC2 and ground-based photometry of about one hundred GCs to derive median and extreme colours, and magnitudes of stars along the HB. They used isochrones and horizontal branch evolutionary models to transform these colors into median and extreme masses of stars on the HB and adopted the median mass loss ($\Delta M_{\text{median}} = M_{\text{RGB}} - M_{\text{median}}$) and the difference between the median and the minimum HB masses ($\delta M = M_{\text{median}} - M_{\text{min}}$) (where M_{RGB} , M_{median} , and M_{min} are RGB, median, and minimum HB masses, respectively) as parameters of the HB morphology. To determine ΔM_{median} and δM , Gratton et al. (2010) assumed for each cluster the value of metallicity and age from Carretta et al. (2009). They find that the median mass loss

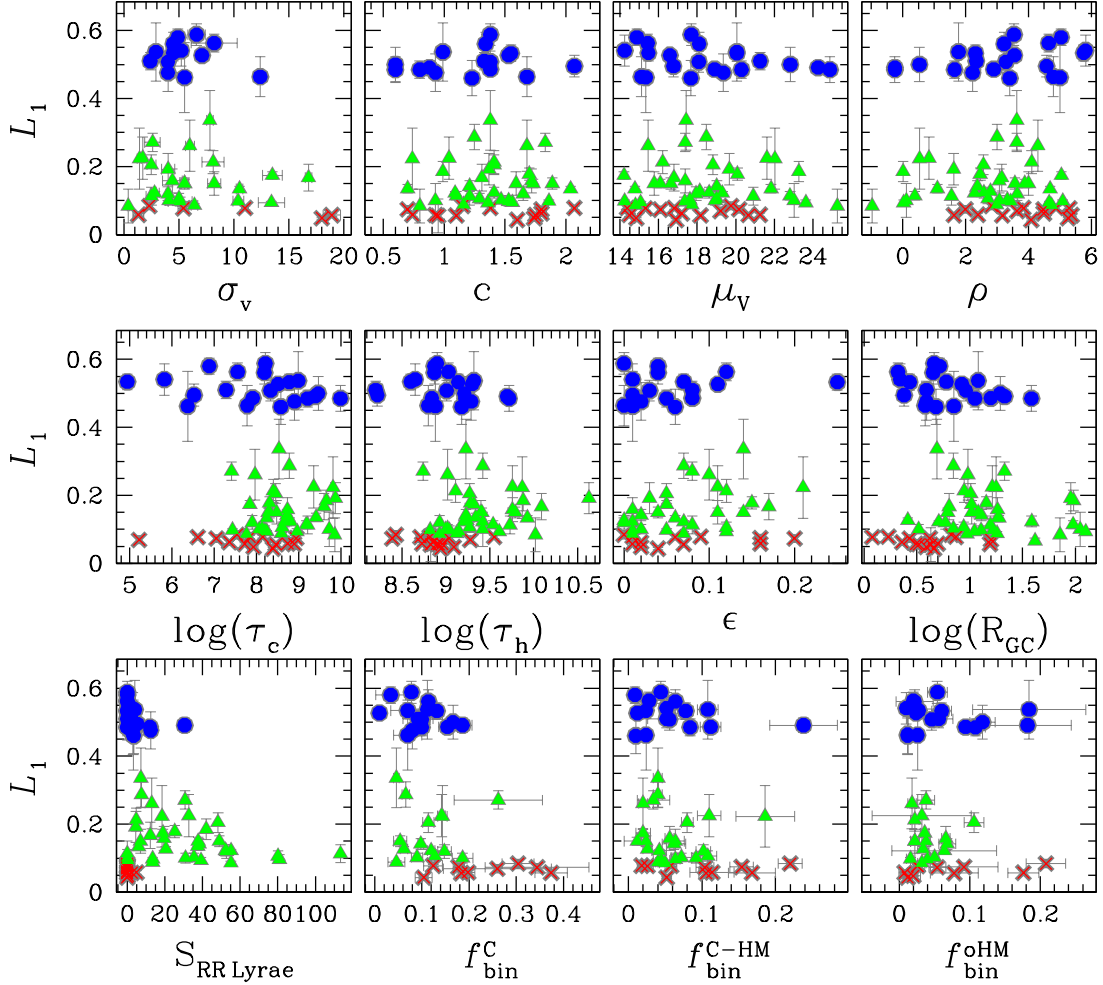


Fig. 9.— L_1 as a function of some parameters of the host GCs. From the left to the right: central velocity dispersion, King (1962) model central concentration, central luminosity brightness, and central luminosity (top), density, core and half mass relaxation time, GC ellipticity, and logarithm of Galactocentric distance (middle), frequency of binaries, and fraction of binaries in the core, in the region between the core and the half-mass radius, and outside the half-mass radius (bottom). σ_v is given in km s^{-1} , μ_v in V magnitude per square arcsecond, τ_c and τ_h in years, and R_{GC} in kpc.

correlates with metallicity and suggest that, if the mass-loss law they used is universal, age is the 2ndP. They conclude that age can explain the behaviour of the median HB when it is coupled with a given mass-loss law that is a linear function of $[\text{Fe}/\text{H}]$. Gratton et al. also suggest that at least

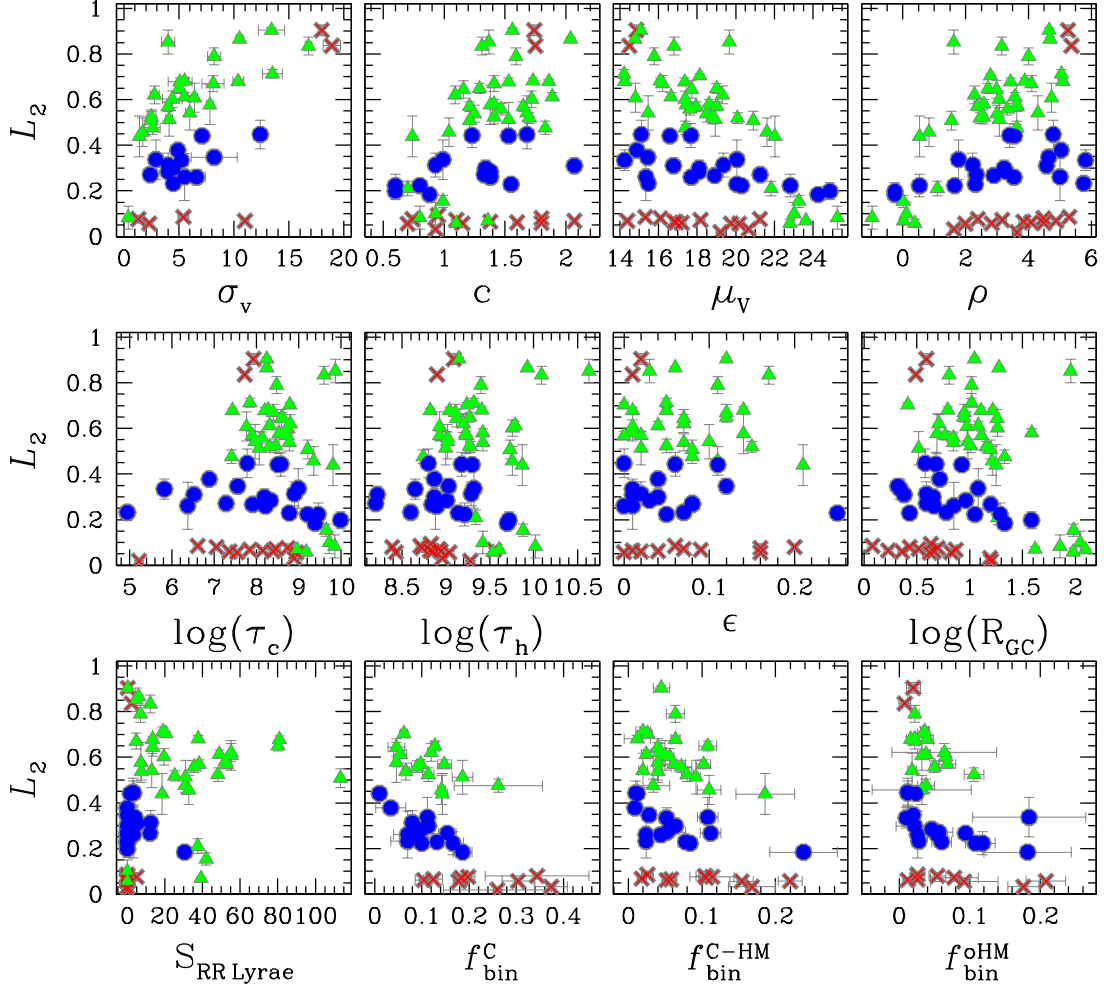


Fig. 10.— L_2 as a function of the same parameters of the host GCs as used in Fig. 9.

another parameter is needed to explain the HB morphology in GCs and argue that He abundance is the most likely candidate. They show that star-to-star helium variations, when combined with a small random quantity, can reproduce the HB morphology, thus supporting the results of other authors (e.g. D’Antona et al. 2002; D’Antona & Caloi 2008; Dalessandro et al. 2013). They find that the HB extension correlates with the interquartile of the Na-O anticorrelation, as previously noticed by the same group of authors (Carretta et al. 2007). Figures 11 and 12 show that δM correlates with L_2 in G2 and G3 GCs, while there is no significant correlation between L_2 and ΔM_{median} . The relation between L_1 and ΔM_{median} is similar to that of L_1 and $[\text{Fe}/\text{H}]$. This reflects

the tight correlation between ΔM_{median} and metallicity.

Fusi-Pecchi et al. (1993) analysed 53 GCs and found that the net length (L_t) of the HB and the presence and extent of blue tails are correlated with the GC density and concentrations, with more concentrated or denser GCs having bluer and longer HB morphologies. A correlation between HB morphology and absolute magnitude has been also detected by Recio-Blanco et al. (2006) who analysed the CMDs of 54 GCs obtained from homogeneous *HST* Wide Field Planetary Camera 2 data (Piotto et al. 2002) and concluded that the maximum effective temperature ($T_{\text{eff,MAX}}$) encountered along the HB correlates with M_V , with more-luminous GCs having also more-extended HBs.

As discussed in Sect. 1, the way an HB morphology metric is defined influences the outcome. It explains why some studies conclude that mass and/or He content are the main driver of HB morphology, while others indicate age as the main 2ndP. The definition of the two parameters $L1$ and $L2$ and their comparison with other quantities commonly used to parametrize the HB morphology (like L_t , $T_{\text{eff,MAX}}$, and $\Delta(V - I)$) may help to shed some light on this controversy. Figure 11 shows that on the one hand there is no significant correlation between either L_t or $T_{\text{eff,MAX}}$ and $L1$. On the other hand, among G2 GCs, $L1$ correlates with $\Delta(V - I)$ among G2 GCs and G3 GCs have, on average, larger $L1$ values than G2 GCs (indicative of older ages in G3 than G2). From Fig. 12 we note that $L2$ correlates with $T_{\text{eff,MAX}}$ for both G2 and G3 GCs and a correlation between $L2$ and L_t is also observed for G2 GCs. Figure 12 reveals no significant correlation between $L2$ and $\Delta(V - I)$. Finally, in Fig. 13 we compare the two parameters introduced in this paper, and show that $L2$ and $L1$ are not significantly correlated.

We conclude that both the metric defined by Fusi-Pecchi et al. (1993) and Recio-Blanco et al. (2006), as well as $L2$, are sensitive to some properties (possibly helium variations) of the HB morphology but lack sensitivity to others (such as age). In contrast $\Delta(V - I)$ and $L1$ are more sensitive to different properties of the HB (e.g. metallicity and age). The use of a pair of parameters, such as $L1$ and $L2$, can provide a more exhaustive description of the HB morphology than one alone.

7. Summary and conclusions

In this paper we exploit both recent observational findings and ideas provided in the early 1980s to investigate the relation between HB morphology and various properties in GCs. These new findings come from studies on multiple stellar populations in GCs that show that the position of a star along the HB is connected to its chemical composition. First generation stars populate the cooler side of the HB and second generation (He-enriched) stars populate the hotter side.

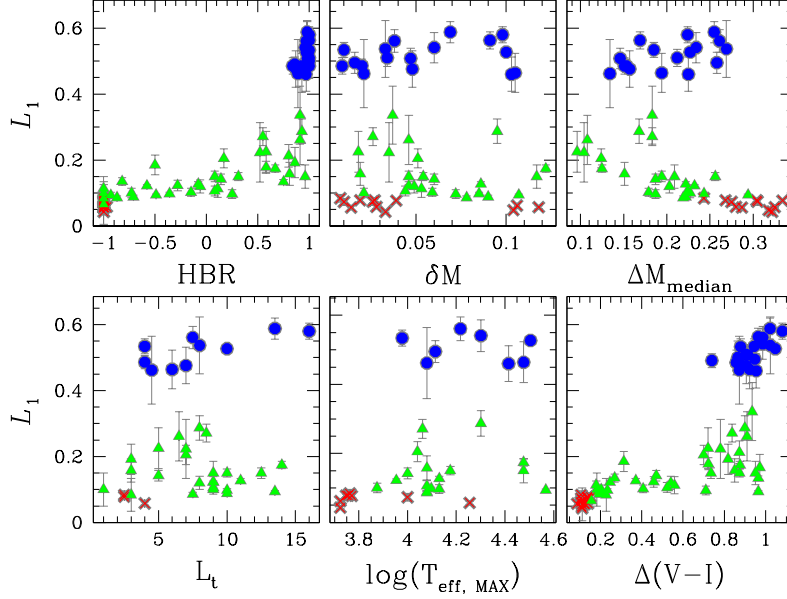


Fig. 11.— L_1 as a function of several quantities used to parametrize HB morphology. Total length of the HB from Fusi-Pecchi et al. (1993, lower-left panel) logarithm of the maximum temperature along the HB from Recio-Blanco et al. (2006, lower-middle panel), Median HB color ($\Delta(V - I)$) from Dotter et al. (2010, lower-right panel), HBR ratio (upper-left panel), maximum and median mass loss from Gratton et al. (2010, upper-middle and upper-right panel).

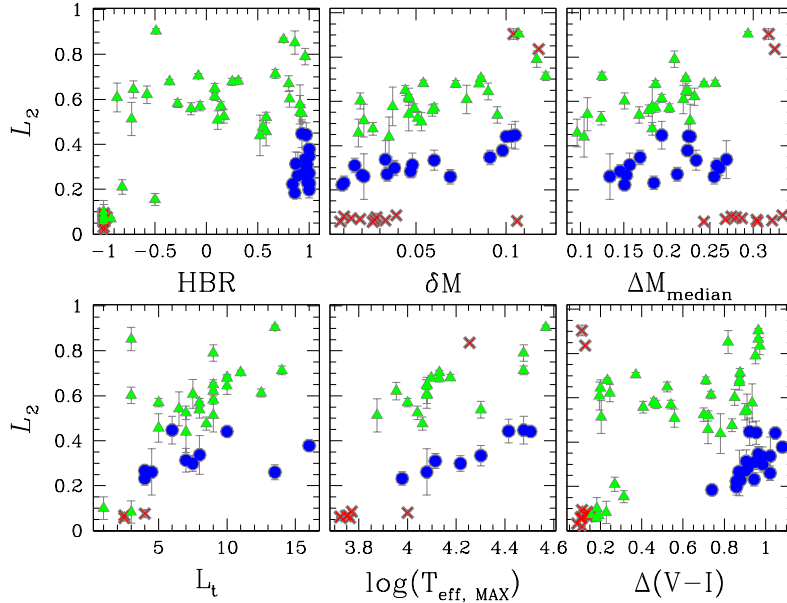


Fig. 12.— As in Fig. 11, but for L_2 .

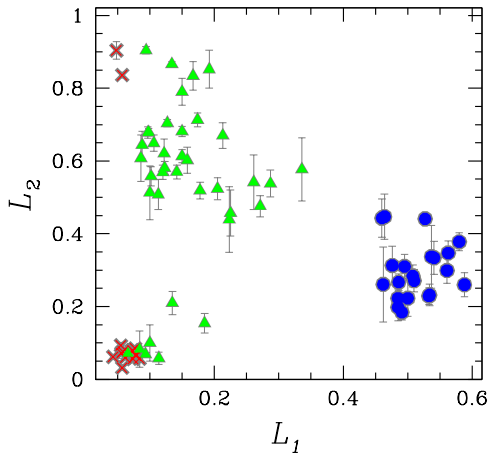


Fig. 13.— L_2 as a function of L_1 for the 74 GCs studied in this paper.

Freeman & Norris (1981) suggested that, apart from metallicity, at least two parameters are needed to explain the HB morphology. One of these should be a *global* parameter that varies from GC to GC, and the other a *non-global* parameter that varies within the GC. Driven by this idea we defined two new parameters to describe the HB morphology: L_1 , which indicates the distance between the RGB and the coolest part of the HB, and L_2 , which measures the color extension of the HB. Our analysis reveals that L_1 depends on GC age and metallicity, while L_2 correlates with the GC luminosity (hence, the mass) and the range of He content (ΔY).

These results suggest that, along the lines suggested by Freeman & Norris, age and metallicity are the main *global* parameters of the HB morphology of GCs, while GC mass is related to the HB extension. Works on multiple stellar populations in GCs show that more massive GCs exhibit, on average, larger internal helium variations, ΔY , than less massive GCs. ΔY is positively correlated with L_2 and GC mass, though this analysis is limited to a small number of GCs at present. This makes it very tempting to suggest that internal star-to-star helium variation, associated with GC mass and the presence of multiple populations, is the main *non-global* parameter.⁸ The use of two quantities L_1 and L_2 , that share a common definition (Sect. 3) but are sensitive to different phenomena allow us to discriminate the effects of global and non-global parameters on the HB morphology.

We thank F. D’Antona and J. Lattanzio for useful discussion and suggestion. We are grate-

⁸If this scenario is correct, in some metal-intermediate GCs with very small L_2 values, like AM 1, Eridanus, Pal 3, Pal 4, Pal 14, Rup 106, and Pyxis, any internal helium variation, if present, should be very small. These GCs are hence good candidates to host a simple stellar population.

full to P. Stetson for providing unpublished light curves of RR Lyrae. APM, JEN, and HJ acknowledge the financial support from the Australian Research Council through Discovery Project grant DP120100475. JEN is also supported by the Australian Research Council through Discovery Project grant DP0984924. AD acknowledges support from the Australian Research Council (grant FL110100012). GP and SC acknowledge financial support from PRIN MIUR 2010-2011, project ‘The Chemical and Dynamical Evolution of the Milky Way and Local Group Galaxies’, prot. 2010LY5N2T, and from PRIN-INAF 2011 ‘Multiple Populations in Globular Clusters: their role in the Galaxy assembly’. Support for this work has been provided by the IAC (grant 310394), and the Education and Science Ministry of Spain (grants AYA2007-3E3506, and AYA2010-16717).

A1. The impact of the RR Lyrae phase on $L1$ and $L2$ measurements.

To investigate the impact of excluding RR Lyrae that might be out of the instability strip in the determination of $L1$ and $L2$, we have simulated a number of CMDs for different choices of the fraction of RR Lyrae (f_V), red-HB (f_R), and blue-HB (f_B) stars. We assumed that RR Lyrae are distributed along the whole instability strip and that all the RR Lyrae ab have the same light curve (this corresponds to the light-curve observed for V27 in M4, $P \sim 0.612d$, and is one of the RR Lyrae ab in M4). We assumed for all the RR Lyrae c the light curve of V40 in M4, $P \sim 0.299d$. The reason why we have chosen these two RR Lyrae is that their amplitude and period are typical of RR Lyrae ab and c. The light curves have been kindly provided by Peter Stetson. They are based on more than 1,000 observations in B , V , and R bands and have been converted into F606W and F814W by using the color-temperature relations by Dotter et al. (2008). We choose V40, for which we have a light curve with the largest amplitude available to us, to maximize possible effects on the determination of $L1$ and $L2$.

F606W and F814W magnitudes have been simulated at different phases to account for the fact that F606W and F814W images are taken at different times. We assumed $f_R = N \times (f_B + f_R)$, ($N = 0, 0.04, 0.10, 0.50, 0.90, 0.96, 1.0$); $f_V = M \times (f_B + f_R + f_V)$, ($M = 0, 0.10, 0.25, 0.50$) and simulated 1,000 CMDs for each combination of f_B , f_V , f_R . For each CMD we have calculated $L1_I$, $L2_I$ and $L1_{II}$, $L2_{II}$. These are the values of $L1$ and $L2$ obtained when all RR Lyrae lie within the instability strip, and when RR Lyrae are at random phase, respectively. The differences $\Delta L1 = L1_I - L1_{II}$ and $\Delta L2 = L2_I - L2_{II}$ are maximal in the case of a HB made of RR Lyrae only ($\Delta L1 = 0.10$, $\Delta L2 = 0.22$). Large difference are also detected in the case of an HB with a very small fraction of red HB stars and a large fraction of RR Lyrae variables ($f_R = 0$ or $f_R = 0.04$). We obtain $\Delta L1 = \Delta L2 \sim 0.08$ when assuming $f_V = 0.50$; $\Delta L1 = \Delta L2 \sim 0.04$ for $f_V = 0.25$; and $\Delta L1 = \Delta L2 \sim 0.01$ for $f_V = 0.1$. We obtain similar results for $\Delta L2$, and $\Delta L1 \sim 0$ when the blue HB hosts a very small fraction of stars ($f_B = 0$ and $f_B = 0.04$). $\Delta L1$ and $\Delta L2$ get closer to zero for larger values of f_B and f_R .

According to the literature values (Lee et al. 1994, Harris 1996, 2010, Gratton et al. 2010

and references therein), extreme cases of $f_V \geq 0.25$ and $f_R \leq 0.1$ are not present among the clusters studied in this paper, which suggests that any error related to the RR Lyrae phase should be smaller than ~ 0.03 - 0.04 mag.

As a further test, for each GC studied in this paper we assumed the corresponding values of f_B , f_V , f_R (Lee et al. 1994, and Harris 1996, 2003 version, and references therein) and simulated 10,000 CMDs. For most GCs we found $\Delta L1 < 0.02$ and $\Delta L2 < 0.02$; $\Delta L1$ is greater than 0.03 mag only in a few GCs, namely NGC 4590, NGC 7078, and NGC 5466. $\Delta L2$ exceeds 0.03 mag also in the cases of Pal 3 and Rup 106. Both $\Delta L1$ and $\Delta L2$ never exceed 0.04 mag. Our tests suggest that the uncertainties on $L1$ and $L2$ measurements due to the random phase of RR Lyrae should be negligible for our purposes. This conclusion is similar to that of Gratton et al. (2010) who showed that RR Lyrae should not affect the determination of the median colors of HB stars.

REFERENCES

- Alves-Brito, A., Yong, D., Meléndez, J., Vásquez, S., & Karakas, A. I. 2012, *A&A*, 540, A3
- Anderson, J., Sarajedini, A., Bedin, L. R., et al. 2008, *AJ*, 135, 2055
- Arp, H. C., Baum, W. A., & Sandage, A. R. 1952, *AJ*, 57, 4
- Bellini, A., Bedin, L. R., Piotto, G., et al. 2010, *AJ*, 140, 631
- Bellini, A., Piotto, G., Milone, A. P., et al. 2013, *ApJ*, 765, 32
- Caloi, V. & D’Antona, F. 2008, *ApJ*, 673, 847
- Carretta, E. 2006, *AJ*, 131, 1766
- Carretta, E., Recio-Blanco, A., Gratton, R. G., Piotto, G., & Bragaglia, A. 2007, *ApJ*, 671, L125
- Carretta, E., Bragaglia, A., Gratton, R., D’Orazi, V., & Lucatello, S. 2009, *A&A*, 508, 695
- Carretta, E., Bragaglia, A., Gratton, R. G., et al. 2010a, *A&A*, 520, A95
- Carretta, E., Bragaglia, A., Gratton, R. G., et al. 2010b, *A&A*, 516, A55
- Cassisi, S., Salaris, M., Pietrinferni, A., et al. 2008, *ApJ*, 672, L115
- Cassisi, S., Salaris, M., Pietrinferni, A. 2012, arXiv:1212.6839
- Catelan, M. 2000, *ApJ*, 531, 826

- Catelan, M. 2009, *Ap&SS*, 320, 261
- Catelan, M. & de Freitas Pacheco, J. A. 1993, *AJ*, 106, 1858
- Dalessandro, E., Salaris, M., Ferraro, F. R., Mucciarelli, A., & Cassisi, S. 2013, *MNRAS*, 430, 459
- D’Antona, F., & Caloi, V. 2008, *MNRAS*, 390, 693
- D’Antona, F., Bellazzini, M., Caloi, V., et al. 2005, *ApJ*, 631, 868
- D’Antona, F., Caloi, V., Montalbán, J., Ventura, P., & Gratton, R. 2002, *A&A*, 395, 69
- De Angeli, F., Piotto, G., Cassisi, S., et al. 2005, *AJ*, 130, 116
- di Criscienzo, M., Ventura, P., D’Antona, F., Milone, A., & Piotto, G. 2010, *MNRAS*, 408, 999
- di Criscienzo, M., D’Antona, F., Milone, A. P., et al. 2011, *MNRAS*, 414, 3381
- Djorgovski, S. & Meylan, G. 1994, *AJ*, 108, 1292
- Dotter, A., Sarajedini, A., & Anderson, J. 2011, *ApJ*, 738, 74
- Dotter, A., Sarajedini, A., Anderson, J., et al. 2010, *ApJ*, 708, 698
- Dotter, A., Chaboyer, B., Jevremović, D., et al. 2008, *ApJS*, 178, 89
- Ferraro, F. R., Paltrinieri, B., Pecci, F. F., Rood, R. T., & Dorman, B. 1998, *ApJ*, 500, 311
- Freeman, K. C. & Norris, J. 1981, *ARA&A*, 19, 319
- Fusi Pecci, F., Ferraro, F. R., Bellazzini, M., et al. 1993, *AJ*, 105, 1145
- Fusi Pecci, F. & Renzini, A. 1978, in *IAU Symposium, Vol. 80, The HR Diagram - The 100th Anniversary of Henry Norris Russell*, ed. A. G. D. Philip & D. S. Hayes, 225
- Gratton, R. G., Carretta, E., Bragaglia, A., Lucatello, S., & D’Orazi, V. 2010, *A&A*, 517, A81
- Gratton, R. G., Lucatello, S., Carretta, E., et al. 2011, *A&A*, 534, A123
- Gratton, R. G., Lucatello, S., Carretta, E., et al. 2012, *A&A*, 539, A19
- Gratton, R. G., Lucatello, S., Sollima, A., et al. 2013, *A&A*, 549, A41
- Harris, W. E. 1996, *AJ*, 112, 1487
- Iben, I. 1968, *Nature*, 220, 143

- King, I. 1962, *AJ*, 67, 471
- King, I. R., Bedin, L. R., Cassisi, S., et al. 2012, *AJ*, 144, 5
- Leaman, R., Vandenberg, D. A., & Mendel, J. T. 2013, arXiv:1309.0822
- Lee, Y.-W., Demarque, P., & Zinn, R. 1994, *ApJ*, 423, 248
- Lind, K., Charbonnel, C., Decressin, T., et al. 2011, *A&A*, 527, A148
- Lovisi, L., Mucciarelli, A., Lanzoni, B., et al. 2012, *ApJ*, 754, 91
- Marín-Franch, A., Aparicio, A., Piotto, G., et al. 2009, *ApJ*, 694, 1498
- Marino, A. F., Milone, A. P., & Lind, K. 2013, *ApJ*, 768, 27
- Marino, A. F., Milone, A. P., Przybilla, N., et al. 2013, *MNRAS*, 2693
- Marino, A. F., Milone, A. P., Piotto, G., et al. 2009, *A&A*, 505, 1099
- Marino, A. F., Milone, A. P., Sneden, C., et al. 2012, *A&A*, 541, A15
- Marino, A. F., Sneden, C., Kraft, R. P., et al. 2011a, *A&A*, 532, A8
- Marino, A. F., Villanova, S., Milone, A. P., et al. 2011b, *ApJ*, 730, L16
- Marino, A. F., Villanova, S., Piotto, G., et al. 2008, *A&A*, 490, 625
- Mengel, J. G. & Gross, P. G. 1976, *Ap&SS*, 41, 407
- Milone, A. P., Bedin, L. R., Piotto, G., et al. 2008, *ApJ*, 673, 241
- Milone, A. P., Marino, A. F., Piotto, G., et al. 2013, *ApJ*, 767, 120
- Milone, A. P., Marino, A. F., Piotto, G., et al. 2012a, *ApJ*, 745, 27
- Milone, A. P., Piotto, G., Bedin, L. R., et al. 2012b, *A&A*, 540, A16
- Milone, A. P., Piotto, G., Bedin, L. R., et al. 2012c, *A&A*, 537, A77
- Milone, A. P., Piotto, G., Bedin, L. R., et al. 2012d, *ApJ*, 744, 58
- Monelli, M., Milone, A. P., Stetson, P. B., et al. 2013, *MNRAS*, 431, 2126
- Norris, J. 1981, *ApJ*, 248, 177
- Norris, J. 1983, *ApJ*, 272, 245

- Norris, J. 1987, *ApJ*, 313, L65
- Norris, J., Cottrell, P. L., Freeman, K. C., & Da Costa, G. S. 1981, *ApJ*, 244, 205
- Peterson, R. C. 1982, *ApJ*, 258, 499
- Piotto, G., King, I. R., Djorgovski, S. G., et al. 2002, *A&A*, 391, 945
- Piotto, G., Bedin, L. R., Anderson, J., et al. 2007, *ApJ*, 661, L53
- Piotto, G., Milone, A. P., Anderson, J., et al. 2012, *ApJ*, 760, 39
- Piotto, G., Milone, A. P., Marino, A. F., et al. 2013, arXiv:1306.5795
- Recio-Blanco, A., Aparicio, A., Piotto, G., de Angeli, F., & Djorgovski, S. G. 2006, *A&A*, 452, 875
- Rood, R. T. & Seitzer, P. O. 1981, in *IAU Colloq. 68: Astrophysical Parameters for Globular Clusters*, ed. A. G. D. Philip & D. S. Hayes, 369
- Rosenberg, A., Saviane, I., Piotto, G., & Aparicio, A. 1999, *AJ*, 118, 2306
- Salaris, M., Riello, M., Cassisi, S., & Piotto, G. 2004, *A&A*, 420, 911
- Sandage, A. & Wallerstein, G. 1960, *ApJ*, 131, 598
- Sandage, A. & Wildey, R. 1967, *ApJ*, 150, 469
- Sarajedini, A., Bedin, L. R., Chaboyer, B., et al. 2007, *AJ*, 133, 1658
- Searle, L. & Zinn, R. 1978, *ApJ*, 225, 357
- Shetrone, M. D. & Keane, M. J. 2000, *AJ*, 119, 840
- Siess, L. & Livio, M. 1999, *MNRAS*, 308, 1133
- Smith, G. H. & Mateo, M. 1990, *ApJ*, 353, 533
- Smith, G. H. & Norris, J. E. 1993, *AJ*, 105, 173
- Snedden, C., Kraft, R. P., Guhathakurta, P., Peterson, R. C., & Fulbright, J. P. 2004, *AJ*, 127, 2162
- Sirianni, M., Jee, M. J., Benítez, N., et al. 2005, *PASP*, 117, 1049
- Soker, N. 1998, *AJ*, 116, 1308
- Stetson, P. B., Bolte, M., Harris, W. E., et al. 1999, *AJ*, 117, 247

van den Bergh, S. 1965, JRASC, 59, 151

van den Bergh, S. 1967, AJ, 72, 324

Vandenberg, D. A., Brogaard, K., Leaman, R., & Casagrande, L., 2013, arXiv:1308.2257

Ventura, P., & D’Antona, F. 2005, ApJ, 635, L149

Ventura, P., Caloi, V., D’Antona, F., et al. 2009, MNRAS, 399, 934

Villanova, S., Geisler, D., & Piotto, G. 2010, ApJ, 722, L18

Villanova, S., Piotto, G., & Gratton, R. G. 2009, A&A, 499, 755

Yong, D., Grundahl, F., D’Antona, F., et al. 2009, ApJ, 695, L62

Yong, D., Grundahl, F., Johnson, J. A., & Asplund, M. 2008, ApJ, 684, 1159

ID	P_A	P_B	P_C	$L1$	$L2$	group
AM 1	0.558±0.003	0.627±0.003	0.720±0.006	0.093±0.007	0.069±0.004	G2
ARP 2	0.105±0.013	0.289±0.020	0.780±0.003	0.491±0.021	0.184±0.021	G3
ERIDANUS	0.584±0.011	0.642±0.005	0.755±0.011	0.111±0.009	0.058±0.012	G2
IC 4499	0.307±0.031	0.815±0.024	0.928±0.008	0.113±0.026	0.508±0.041	G2
LYNGA 7	1.387±0.008	1.480±0.003	1.534±0.004	0.055±0.050	0.093±0.009	G1

Table 1: Horizontal Branch parameters.

ID	ΔY	Reference
NGC 104 (47 Tuc)	~0.03	di Criscienzo et al. (2010), Milone et al. (2012d)
NGC 288	0.013±0.001	Piotto et al. (2013)
NGC 2419	~0.17	di Criscienzo et al. (2011)
NGC 2808	~0.14	Milone et al. (2012c)
NGC 5139 (ω Cen)	0.14±0.01	King et al. (2012)
NGC 6397	~0.01	Milone et al. (2012a)*
NGC 6441	~0.07	Bellini et al. (2013)
NGC 6752	0.035±0.012	Milone et al. (2013)
NGC 7078	0.053±0.015	Milone et al. (2014, in preparation)

*Accurate analysis of the MS width by di Criscienzo et al. (2010) previously showed that any helium variation in NGC 6397 must be smaller than $\Delta Y \sim 0.02$.

Table 2: Literature estimate of the maximum helium difference between stellar populations based on the analysis of multiple MSs or multiple RGBs.

Parameter	L1				L2			
	G1	G2	G3	G2 + G3	G1	G2	G3	G2 + G3
[Fe/H]	$r = -0.13$ $N=15$ $\sigma_r=0.26$	$r = -0.70$ $N=38$ $\sigma_r=0.08$	$r = 0.42$ $N=21$ $\sigma_r=0.18$	$r = -0.47$ $N=59$ $\sigma_r=0.11$	$r = -0.08$ $N=15$ $\sigma_r=0.31$	$r = 0.19$ $N=38$ $\sigma_r=0.16$	$r = 0.57$ $N=21$ $\sigma_r=0.13$	$r = 0.24$ $N=59$ $\sigma_r=0.13$
M_V	$r = 0.09$ $N=15$ $\sigma_r=0.13$	$r = -0.23$ $N=38$ $\sigma_r=0.16$	$r = -0.08$ $N=21$ $\sigma_r=0.24$	$r = 0.09$ $N=59$ $\sigma_r=0.13$	$r = -0.57$ $N=15$ $\sigma_r=0.23$	$r = -0.89$ $N=38$ $\sigma_r=0.05$	$r = -0.71$ $N=21$ $\sigma_r=0.13$	$r = -0.80$ $N=59$ $\sigma_r=0.06$
AGE_{D10}	$r = 0.35$ $N=15$ $\sigma_r=0.20$	$r = 0.76$ $N=37$ $\sigma_r=0.08$	$r = -0.22$ $N=21$ $\sigma_r=0.20$	$r = 0.72$ $N=58$ $\sigma_r=0.08$	$r = 0.23$ $N=15$ $\sigma_r=0.29$	$r = 0.28$ $N=37$ $\sigma_r=0.18$	$r = -0.07$ $N=21$ $\sigma_r=0.24$	$r = -0.06$ $N=58$ $\sigma_r=0.16$
AGE_{MF09}	$r = 0.38$ $N=15$ $\sigma_r=0.26$	$r = 0.47$ $N=26$ $\sigma_r=0.18$	$r = -0.05$ $N=20$ $\sigma_r=0.20$	$r = 0.38$ $N=46$ $\sigma_r=0.15$	$r = 0.30$ $N=15$ $\sigma_r=0.30$	$r = -0.29$ $N=26$ $\sigma_r=0.16$	$r = 0.17$ $N=20$ $\sigma_r=0.22$	$r = -0.30$ $N=46$ $\sigma_r=0.14$
AGE_{DA05}	$r = 0.60$ $N=5$ $\sigma_r=0.37$	$r = 0.72$ $N=25$ $\sigma_r=0.13$	$r = -0.32$ $N=11$ $\sigma_r=0.36$	$r = 0.57$ $N=36$ $\sigma_r=0.13$	$r = -0.60$ $N=5$ $\sigma_r=0.40$	$r = -0.50$ $N=25$ $\sigma_r=0.14$	$r = 0.03$ $N=11$ $\sigma_r=0.36$	$r = -0.49$ $N=36$ $\sigma_r=0.13$
AGE_{V13}	$r = 0.62$ $N=12$ $\sigma_r=0.20$	$r = 0.73$ $N=31$ $\sigma_r=0.09$	$r = -0.21$ $N=18$ $\sigma_r=0.25$	$r = 0.68$ $N=49$ $\sigma_r=0.10$	$r = 0.62$ $N=12$ $\sigma_r=0.21$	$r = 0.01$ $N=31$ $\sigma_r=0.20$	$r = -0.22$ $N=18$ $\sigma_r=0.25$	$r = -0.34$ $N=49$ $\sigma_r=0.16$
AGE_{D10}^*	$r = 0.35$ $N=14$ $\sigma_r=0.20$	$r = 0.76$ $N=34$ $\sigma_r=0.08$	$r = -0.22$ $N=21$ $\sigma_r=0.20$	$r = 0.74$ $N=55$ $\sigma_r=0.07$	$r = 0.39$ $N=14$ $\sigma_r=0.26$	$r = 0.30$ $N=34$ $\sigma_r=0.19$	$r = -0.08$ $N=21$ $\sigma_r=0.24$	$r = -0.08$ $N=55$ $\sigma_r=0.17$
AGE_{MF09}^*	$r = 0.41$ $N=14$ $\sigma_r=$	$r = 0.40$ $N=23$ $\sigma_r=0.21$	$r = -0.05$ $N=20$ $\sigma_r=0.20$	$r = 0.33$ $N=43$ $\sigma_r=0.16$	$r = 0.31$ $N=14$ $\sigma_r=0.30$	$r = -0.29$ $N=23$ $\sigma_r=0.16$	$r = 0.17$ $N=20$ $\sigma_r=0.22$	$r = -0.30$ $N=43$ $\sigma_r=0.14$
AGE_{DA05}^*	$r = 0.60$ $N=5$ $\sigma_r=0.37$	$r = 0.71$ $N=23$ $\sigma_r=0.14$	$r = -0.32$ $N=11$ $\sigma_r=0.36$	$r = 0.53$ $N=34$ $\sigma_r=0.15$	$r = -0.60$ $N=5$ $\sigma_r=0.40$	$r = -0.53$ $N=23$ $\sigma_r=0.14$	$r = 0.03$ $N=11$ $\sigma_r=0.36$	$r = -0.47$ $N=34$ $\sigma_r=0.13$
AGE_{V13}^*	$r = 0.62$ $N=12$ $\sigma_r=0.20$	$r = 0.70$ $N=28$ $\sigma_r=0.10$	$r = -0.21$ $N=18$ $\sigma_r=0.25$	$r = 0.65$ $N=46$ $\sigma_r=0.10$	$r = 0.62$ $N=12$ $\sigma_r=0.21$	$r = 0.07$ $N=28$ $\sigma_r=0.22$	$r = -0.22$ $N=18$ $\sigma_r=0.25$	$r = -0.32$ $N=46$ $\sigma_r=0.16$
$\log(\Delta Y)$	— $N=2$ —	$r = -0.30$ $N=5$ $\sigma_r=0.54$	— $N=2$ —	$r = -0.71$ $N=7$ $\sigma_r=0.31$	— $N=2$ —	$r = 0.70$ $N=5$ $\sigma_r=0.37$	— $N=2$ —	$r = 0.89$ $N=7$ $\sigma_r=0.17$
σ_V	$r = -0.54$ $N=6$ $\sigma_r=0.38$	$r = -0.07$ $N=7$ $\sigma_r=0.22$	$r = 0.10$ $N=13$ $\sigma_r=0.30$	$r = -0.02$ $N=38$ $\sigma_r=0.15$	$r = 0.66$ $N=6$ $\sigma_r=0.29$	$r = 0.79$ $N=7$ $\sigma_r=0.12$	$r = 0.40$ $N=13$ $\sigma_r=0.28$	$r = 0.46$ $N=38$ $\sigma_r=0.14$
c	$r = 0.13$ $N=14$ $\sigma_r=0.25$	$r = 0.08$ $N=34$ $\sigma_r=0.17$	$r = 0.26$ $N=16$ $\sigma_r=0.23$	$r = -0.10$ $N=50$ $\sigma_r=0.14$	$r = 0.07$ $N=14$ $\sigma_r=0.31$	$r = 0.54$ $N=34$ $\sigma_r=0.14$	$r = 0.52$ $N=16$ $\sigma_r=0.23$	$r = 0.55$ $N=50$ $\sigma_r=0.10$
μ_V	$r = -0.01$ $N=14$ $\sigma_r=0.28$	$r = -0.07$ $N=37$ $\sigma_r=0.18$	$r = -0.23$ $N=21$ $\sigma_r=0.23$	$r = -0.07$ $N=58$ $\sigma_r=0.14$	$r = -0.65$ $N=14$ $\sigma_r=0.21$	$r = -0.76$ $N=37$ $\sigma_r=0.10$	$r = -0.68$ $N=21$ $\sigma_r=0.15$	$r = -0.57$ $N=58$ $\sigma_r=0.11$
ρ	$r = -0.09$ $N=14$ $\sigma_r=0.26$	$r = 0.05$ $N=37$ $\sigma_r=0.18$	$r = 0.29$ $N=21$ $\sigma_r=0.21$	$r = 0.14$ $N=58$ $\sigma_r=0.14$	$r = 0.69$ $N=14$ $\sigma_r=0.18$	$r = 0.69$ $N=37$ $\sigma_r=0.12$	$r = 0.56$ $N=21$ $\sigma_r=0.19$	$r = 0.47$ $N=58$ $\sigma_r=0.13$
$\log(\tau_c)$	$r = -0.31$ $N=14$ $\sigma_r=0.21$	$r = 0.09$ $N=37$ $\sigma_r=0.18$	$r = -0.28$ $N=21$ $\sigma_r=0.20$	$r = -0.21$ $N=58$ $\sigma_r=0.13$	$r = -0.15$ $N=14$ $\sigma_r=0.32$	$r = -0.35$ $N=37$ $\sigma_r=0.18$	$r = -0.8$ $N=21$ $\sigma_r=0.23$	$r = -0.20$ $N=58$ $\sigma_r=0.15$
$\log(\tau_h)$	$r = -0.29$ $N=15$ $\sigma_r=0.28$	$r = 0.19$ $N=37$ $\sigma_r=0.18$	$r = -0.21$ $N=21$ $\sigma_r=0.18$	$r = -0.33$ $N=58$ $\sigma_r=0.13$	$r = -0.28$ $N=15$ $\sigma_r=0.27$	$r = -0.13$ $N=37$ $\sigma_r=0.18$	$r = -0.23$ $N=21$ $\sigma_r=0.24$	$r = 0.08$ $N=58$ $\sigma_r=0.15$
ϵ	$r = -0.10$ $N=12$ $\sigma_r=0.32$	$r = 0.45$ $N=30$ $\sigma_r=0.14$	$r = 0.14$ $N=17$ $\sigma_r=0.27$	$r = 0.07$ $N=47$ $\sigma_r=0.15$	$r = 0.05$ $N=12$ $\sigma_r=0.33$	$r = -0.05$ $N=30$ $\sigma_r=0.20$	$r = -0.16$ $N=17$ $\sigma_r=0.27$	$r = 0.09$ $N=47$ $\sigma_r=0.15$
$\log(R_{GC} [kpc])$	$r = -0.08$ $N=15$ $\sigma_r=0.27$	$r = -0.18$ $N=38$ $\sigma_r=0.16$	$r = -0.29$ $N=21$ $\sigma_r=0.19$	$r = -0.45$ $N=59$ $\sigma_r=0.11$	$r = -0.50$ $N=15$ $\sigma_r=0.22$	$r = -0.44$ $N=38$ $\sigma_r=0.16$	$r = -0.50$ $N=21$ $\sigma_r=0.19$	$r = -0.17$ $N=59$ $\sigma_r=0.15$

* GCs with double SGB excluded from the analysis

Table 3: Spearman’s rank correlation coefficients indicating the statistical dependence between L1 (columns 2-5) L2 (columns 6-9) and several parameters of the host GCs for G1 G2 G3 and

Parameter	L1				L2			
	G1	G2	G3	G2 + G3	G1	G2	G3	G2 + G3
$S_{RR Lyrae}$	$r = -0.01$ $N=14$ $\sigma_r=0.27$	$r = -0.26$ $N=36$ $\sigma_r=0.17$	$r = -0.48$ $N=20$ $\sigma_r=0.17$	$r = -0.66$ $N=56$ $\sigma_r=0.11$	$r = -0.12$ $N=14$ $\sigma_r=0.22$	$r = -0.68$ $N=36$ $\sigma_r=0.19$	$r = -0.51$ $N=20$ $\sigma_r=0.24$	$r = -0.32$ $N=56$ $\sigma_r=0.13$
f_{bin}^C	$r = 0.19$ $N=9$ $\sigma_r=0.40$	$r = -0.03$ $N=16$ $\sigma_r=0.30$	$r = -0.22$ $N=15$ $\sigma_r=0.26$	$r = -0.18$ $N=31$ $\sigma_r=0.18$	$r = -0.12$ $N=9$ $\sigma_r=0.36$	$r = -0.68$ $N=16$ $\sigma_r=0.15$	$r = -0.51$ $N=15$ $\sigma_r=0.25$	$r = -0.32$ $N=31$ $\sigma_r=0.17$
f_{bin}^{C-HM}	$r = -0.09$ $N=11$ $\sigma_r=0.35$	$r = -0.19$ $N=24$ $\sigma_r=0.19$	$r = -0.18$ $N=16$ $\sigma_r=0.29$	$r = -0.15$ $N=40$ $\sigma_r=0.14$	$r = -0.67$ $N=11$ $\sigma_r=0.23$	$r = -0.47$ $N=24$ $\sigma_r=0.20$	$r = -0.56$ $N=16$ $\sigma_r=0.23$	$r = -0.27$ $N=40$ $\sigma_r=0.15$
f_{bin}^{oHM}	$r = 0.49$ $N=11$ $\sigma_r=0.29$	$r = -0.14$ $N=18$ $\sigma_r=0.24$	$r = -0.07$ $N=17$ $\sigma_r=0.28$	$r = -0.02$ $N=35$ $\sigma_r=0.17$	$r = -0.75$ $N=11$ $\sigma_r=0.18$	$r = -0.45$ $N=18$ $\sigma_r=0.21$	$r = -0.69$ $N=17$ $\sigma_r=0.19$	$r = -0.39$ $N=35$ $\sigma_r=0.15$
W_{RGB}	— $N=3$ —	$r = -0.45$ $N=9$ $\sigma_r=0.31$	$r = -0.08$ $N=9$ $\sigma_r=0.35$	$r = -0.23$ $N=18$ $\sigma_r=0.22$	— $N=3$ —	$r = 0.50$ $N=9$ $\sigma_r=0.35$	$r = 0.35$ $N=9$ $\sigma_r=0.37$	$r = 0.30$ $N=18$ $\sigma_r=0.23$
IQR([O/Na])	— $N=4$ —	$r = -0.13$ $N=13$ $\sigma_r=0.26$	$r = 0.00$ $N=8$ $\sigma_r=0.38$	$r = -0.02$ $N=21$ $\sigma_r=0.21$	— $N=4$ —	$r = 0.82$ $N=13$ $\sigma_r=0.13$	$r = 0.90$ $N=8$ $\sigma_r=0.17$	$r = 0.41$ $N=21$ $\sigma_r=0.21$
R_{CN}	— $N=2$ —	$r = 0.29$ $N=11$ $\sigma_r=0.30$	— $N=3$ —	$r = 0.13$ $N=14$ $\sigma_r=0.27$	— $N=2$ —	$r = 0.47$ $N=11$ $\sigma_r=0.24$	— $N=3$ —	$r = 0.38$ $N=14$ $\sigma_r=0.27$
R	$r = 0.07$ $N=8$ $\sigma_r=0.40$	$r = 0.17$ $N=19$ $\sigma_r=0.26$	$r = -0.07$ $N=7$ $\sigma_r=0.39$	$r = 0.11$ $N=26$ $\sigma_r=0.19$	$r = 0.26$ $N=8$ $\sigma_r=0.35$	$r = 0.19$ $N=19$ $\sigma_r=0.24$	$r = -0.32$ $N=7$ $\sigma_r=0.42$	$r = 0.07$ $N=26$ $\sigma_r=0.22$
f_{POPI}	— $N=4$ —	$r = 0.38$ $N=8$ $\sigma_r=0.39$	$r = -0.32$ $N=7$ $\sigma_r=0.36$	$r = -0.03$ $N=15$ $\sigma_r=0.29$	— $N=4$ —	$r = -0.12$ $N=8$ $\sigma_r=0.38$	$r = -0.07$ $N=7$ $\sigma_r=0.36$	$r = -0.02$ $N=15$ $\sigma_r=0.27$
$Y(R')$	$r = -0.27$ $N=11$ $\sigma_r=0.36$	$r = -0.16$ $N=25$ $\sigma_r=0.23$	$r = 0.12$ $N=17$ $\sigma_r=0.28$	$r = 0.07$ $N=42$ $\sigma_r=0.15$	$r = 0.15$ $N=11$ $\sigma_r=0.34$	$r = 0.44$ $N=25$ $\sigma_r=0.21$	$r = -0.06$ $N=17$ $\sigma_r=0.26$	$r = 0.04$ $N=42$ $\sigma_r=0.16$
$L2$	$r = -0.35$ $N=15$ $\sigma_r=0.24$	$r = 0.05$ $N=38$ $\sigma_r=0.17$	$r = 0.10$ $N=21$ $\sigma_r=0.25$	$r = -0.35$ $N=59$ $\sigma_r=0.15$	$r = 1.00$ $N=15$ $\sigma_r=0.00$	$r = 1.00$ $N=38$ $\sigma_r=0.00$	$r = 1.00$ $N=21$ $\sigma_r=0.00$	$r = 1.00$ $N=59$ $\sigma_r=0.00$
HBR	$r = 0.43$ $N=13$ $\sigma_r=0.28$	$r = 0.79$ $N=37$ $\sigma_r=0.07$	$r = 0.48$ $N=21$ $\sigma_r=0.16$	$r = 0.91$ $N=58$ $\sigma_r=0.02$	$r = -0.24$ $N=13$ $\sigma_r=0.27$	$r = 0.44$ $N=37$ $\sigma_r=0.16$	$r = -0.04$ $N=21$ $\sigma_r=0.26$	$r = -0.15$ $N=58$ $\sigma_r=0.17$
δM	$r = -0.48$ $N=12$ $\sigma_r=0.24$	$r = -0.36$ $N=25$ $\sigma_r=0.20$	$r = 0.12$ $N=17$ $\sigma_r=0.29$	$r = -0.19$ $N=42$ $\sigma_r=0.30$	$r = 0.39$ $N=12$ $\sigma_r=0.30$	$r = 0.66$ $N=25$ $\sigma_r=0.14$	$r = 0.80$ $N=17$ $\sigma_r=0.15$	$r = 0.48$ $N=42$ $\sigma_r=0.13$
ΔM_{median}	$r = -0.47$ $N=11$ $\sigma_r=0.28$	$r = -0.68$ $N=24$ $\sigma_r=0.10$	$r = 0.50$ $N=17$ $\sigma_r=0.19$	$r = 0.00$ $N=41$ $\sigma_r=0.17$	$r = 0.39$ $N=11$ $\sigma_r=0.30$	$r = 0.63$ $N=24$ $\sigma_r=0.17$	$r = 0.35$ $N=17$ $\sigma_r=0.22$	$r = 0.14$ $N=41$ $\sigma_r=0.17$
L_t	— $N=4$ —	$r = -0.21$ $N=23$ $\sigma_r=0.19$	$r = 0.68$ $N=11$ $\sigma_r=0.21$	$r = -0.06$ $N=34$ $\sigma_r=0.19$	— $N=4$ —	$r = 0.62$ $N=23$ $\sigma_r=0.17$	$r = 0.38$ $N=11$ $\sigma_r=0.33$	$r = 0.44$ $N=34$ $\sigma_r=0.18$
$\log(T_{eff,MAX})$	$r = 0.10$ $N=8$ $\sigma_r=0.44$	$r = 0.10$ $N=17$ $\sigma_r=0.25$	$r = -0.14$ $N=8$ $\sigma_r=0.34$	$r = 0.27$ $N=25$ $\sigma_r=0.20$	$r = 0.71$ $N=8$ $\sigma_r=0.26$	$r = 0.77$ $N=17$ $\sigma_r=0.16$	$r = 0.90$ $N=8$ $\sigma_r=0.14$	$r = 0.20$ $N=25$ $\sigma_r=0.21$
$\Delta(V - I)$	$r = 0.21$ $N=15$ $\sigma_r=0.26$	$r = 0.66$ $N=38$ $\sigma_r=0.12$	$r = 0.64$ $N=21$ $\sigma_r=0.14$	$r = 0.76$ $N=59$ $\sigma_r=0.08$	$r = 0.49$ $N=15$ $\sigma_r=0.23$	$r = 0.57$ $N=38$ $\sigma_r=0.14$	$r = 0.75$ $N=21$ $\sigma_r=0.14$	$r = 0.10$ $N=59$ $\sigma_r=0.14$

* GCs with double SGB excluded from the analysis

Table 4: Spearman’s rank correlation coefficients indicating the statistical dependence between L1 (columns 2-5), L2 (columns 6-9) and several parameters of the host GCs for G1, G2, G3, and G2+G3 GCs. The values of σ_r , which provide an estimate of the robustness of r measurements, and the numbers of analyzed GCs (N) are also listed.

Author	age_{G2} [Gyr]	age_{G3} [Gyr]
all		
Dotter et al. (2010, 2011)	12.3±0.1	13.2±0.1
Marín-Franch et al. (2009)	12.8±0.2	13.4±0.2
De Angeli et al. (2005)	12.3±0.3	13.2±0.3
VandenBerg et al. (2013) and Leaman et al. (2013)	11.8±0.1	12.5±0.1
metal-rich sample		
Dotter et al. (2010, 2011)	12.1±0.2	12.9±0.3
Marín-Franch et al. (2009)	12.7±0.3	13.3±0.1
De Angeli et al. (2005)	11.6±0.5	12.8±0.1
VandenBerg et al. (2013) and Leaman et al. (2013)	11.4±0.2	12.3±0.5
metal-intermediate sample		
Dotter et al. (2010, 2011)	11.9±0.2	13.0±0.1
Marín-Franch et al. (2009)	12.5±0.3	13.3±0.3
De Angeli et al. (2005)	11.7±0.5	13.0±0.5
VandenBerg et al. (2013) and Leaman et al. (2013)	11.6±0.1	12.2±0.2
metal-poor sample		
Dotter et al. (2010, 2011)	13.1±0.1	13.3±0.1
Marín-Franch et al. (2009)	13.0±0.3	13.4±0.3
De Angeli et al. (2005)	13.5±0.3	14.0±0.5
VandenBerg et al. (2013) and Leaman et al. (2013)	12.4±0.1	12.7±0.1

Table 5: Average ages for G2 and G3 GCs.